FINAL BACHELOR PROJECT

STUDY OF THE DOWNSTREAM AERODYNAMIC ELEMENTS OF CURRENT FORMULA 1 CARS

Student:
José Ramón Estellés Calderón
jose-ramon.estelles-calderon@ipsa.fr
jrestcal@etsid.upv.es

Supervisor:
M. Wafik Abassi
wafik.abassi@ipsa.fr

Co-supervisor:
Mme. Xandra Marcelle Margot
xmargot@mot.upv.es

Institut Polytechnique des Sciences Avancées

June 22, 2023
Paris

Abstract

Formula 1 is a discipline that makes use of sophisticated technology in order to constantly improve the performance of the cars and offer a great sporting spectacle. Much of this performance depends on the aerodynamic surfaces that make up the car, which allow the airflow to be directed in the most efficient way so as to maintain the best possible balance between downforce and drag. This project focuses on a partial analysis of the aerodynamics of current F1 cars, focusing on the airflow downstream of the car. Using 3D modelling software, both the car's floor and its rear part will be recreated, including their associated aerodynamic surfaces. Subsequently, CFD simulations of the flow behaviour as it passes through these surfaces and as it exits the vehicle will be carried out, under the conditions faced by these vehicles when competing on the track. The effects of these devices on car performance will be studied and discussed.

Résumé

La Formule 1 est une discipline qui fait appel à des technologies sophistiquées afin d'améliorer constamment les performances des voitures et d'offrir un grand spectacle sportif. Une grande partie de ces performances dépend des surfaces aérodynamiques qui composent la voiture et qui permettent de diriger le flux d'air de la manière la plus efficace possible afin de maintenir le meilleur équilibre possible entre la force d'appui et la traînée. Ce projet se concentre sur une analyse partielle de l'aérodynamique des voitures de F1 actuelles, en se concentrant sur l'écoulement de l'air en aval de la voiture. À l'aide d'un logiciel de modélisation 3D, le plancher et la partie arrière de la voiture seront recréés, ainsi que les surfaces aérodynamiques qui leur sont associées. Ensuite, des simulations CFD du comportement de l'écoulement lorsqu'il traverse ces surfaces et lorsqu'il sort du véhicule seront effectuées, dans les conditions auxquelles ces véhicules sont confrontés lorsqu'ils concourent sur la piste. Les effets de ces dispositifs sur les performances de la voiture seront étudiés et discutés.

Resumen

La Fórmula 1 es una disciplina que utiliza tecnología sofisticada para mejorar constantemente el rendimiento de los coches y ofrecer un gran espectáculo deportivo. Gran parte de este rendimiento depende de las superficies aerodinámicas que componen el monoplaza, que permiten dirigir el flujo de aire de la manera más eficiente para mantener el mejor equilibrio posible entre carga aerodinámica y resistencia. Este proyecto se centra en un análisis parcial de la aerodinámica de los actuales coches de F1, centrándose en el flujo de aire aguas abajo del monoplaza. Utilizando software de modelado 3D, se recrearán tanto el suelo del coche como su parte trasera, incluyendo sus superficies aerodinámicas asociadas. Posteriormente, se llevarán a cabo simulaciones CFD del comportamiento del flujo a su paso por estas superficies y a su salida del vehículo, en las condiciones a las que se enfrentan estos vehículos cuando compiten en la pista. Se estudiarán y discutirán los efectos de estos dispositivos en el rendimiento de los coches.

Resum

La Fórmula 1 és una disciplina que utilitza tecnologia sofisticada per a millorar constantment el rendiment dels cotxes i oferir un gran espectacle esportiu. Gran part d'aquest rendiment depén de les superfícies aerodinàmiques que componen el monoplaça, que permeten dirigir el flux d'aire de la manera més eficient per a mantindre el millor equilibri possible entre càrrega aerodinàmica i resistència. Aquest projecte se centra en una anàlisi parcial de l'aerodinàmica dels actuals cotxes de F1, centrant-se en el flux d'aire aigües avall del monoplaça. Utilitzant programari de modelatge 3D, es recrearan tant el sòl del cotxe com la seua part posterior, incloent-hi les seues superfícies aerodinàmiques associades. Posteriorment, es duran a terme simulacions CFD del comportament del flux al seu pas per aquestes superfícies i a la seua eixida del vehicle, en les condicions a les quals s'enfronten aquests vehicles quan competeixen en la pista. S'estudiaran i discutiran els efectes d'aquests dispositius en el rendiment dels cotxes.

Contents

List of Figures

1 Context

Formula 1 represents the most popular and prestigious motorsport championship in the world, reasons why it has become the leading international motor racing competition.

This discipline has its roots in France in 1894, where the first "Grand Prix" were held. Back then, these were individual, unconnected events on dirt roads, with virtually no restrictions. The beginning of modern Formula 1 dates back to 1950. Important advances took place in several areas of the vehicle. Aerodynamics slowly gained importance in car design in the late 1960s. At the end of the following decade, in 1977, Lotus introduced a ground effect car, the Lotus 78. This was the first ground effect vehicle in Formula 1 history.

The advantage of this car relied on being provided with sidepods with a reversed airfoil shape. This allowed to create a low pressure zone between the car and the track by means of increasing air velocity, following Bernoulli's principle. To keep this low pressure area and avoid air mass flow from the surrounding areas (with greater pressure) to enter the region, flexible skirts were added to "seal" the laterals of the vehicle with the track. These devices allowed the generation of great downforce. Nevertheless, they resulted to be a threat to pilot's safety. If the underside of the car contacted the ground (for instance, going over a bump or a kerb), the flow under the car would be constricted too much, causing a sudden increase of air pressure and the loss of the ground effect. In addition, the ground effect sometimes led to excessive velocities at turns, which resulted in pilots suffering unsafe G-forces.

As a result, ground effect aerodynamics was banned in 1983, and a rule that required all cars to have flat bottoms was introduced by the FIA (*Federation Internationale de l'Automobile*) in order to stand up for safety in F1 races. This forced teams to develop new ways of achieving underfloor downforce without sidepod venturis or side skirts, becoming diffusers a safe solution for this issue.

The next major aerodynamic changes came up in 2022, when the F1 governing body introduced new rules that intended to promote closer racing through the use of ground effects, larger wheels with low-profile tires, and redesigned nose and wing regulations. With these new rules, from 2022 on, the cars would feature fully shaped underfloor tunnels, rather than flat underfloors, allowing teams to generate large amounts of efficient downforce through ground effect.

2 Aim of the project

The goal that this project pursues is to conduct an aerodynamic analysis of the new elements introduced by the FIA regulations for the 2022 season downstream the F1 vehicle, this is, those located in the rear body of the car. Specifically, three devices are studied: the underfloor, the beam wing and the rear wing (which incorporates the DRS system). The location of these elements in a standard Formula 1 car is depicted in Figure 2.1. The underfloor is highlighted in blue, the beam wing in green and the rear wing in purple.

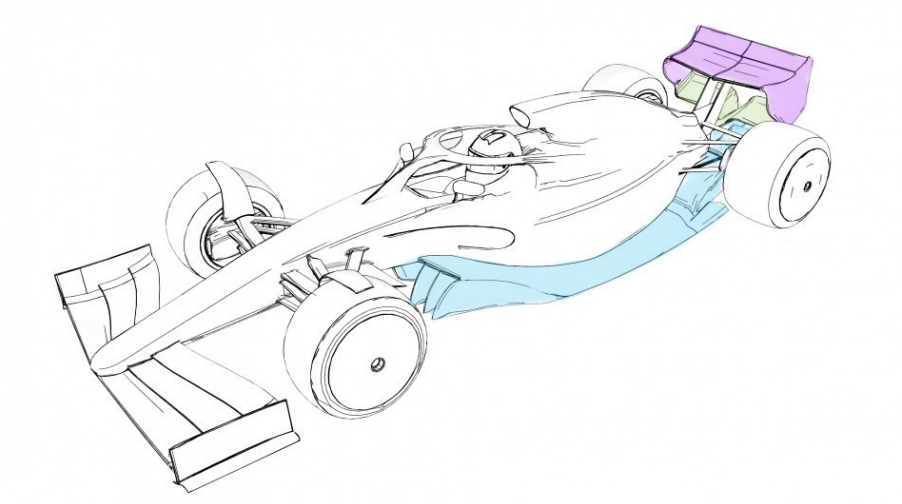

Figure 2.1: Car concept conceived for the 2022 F1 season. [1]

In terms of aerodynamics, there are three forces acting on the car, schematized in Figure 2.2: downforce in vertical direction (in grey), drag in longitudinal direction (in orange) and side forces in lateral direction (in yellow). Among these, downforce is undoubtedly the most important in terms of car performance. As the car travels through the air, the downforce will push the car down into the ground. When downforce levels are reduced, the car slides around more and the rear end is less stable. Having high downforce is specially important for corners, where a better grip and traction are required in order to enter and exit the curve at the greatest possible speed. However, downforce is not as important in straights, where achieving low drag levels is preferable than having the car planted to the track. And this is when the DRS system comes into play. In any case, the design of aerodynamic devices that allow to generate downforce and control drag is essential in Formula 1.

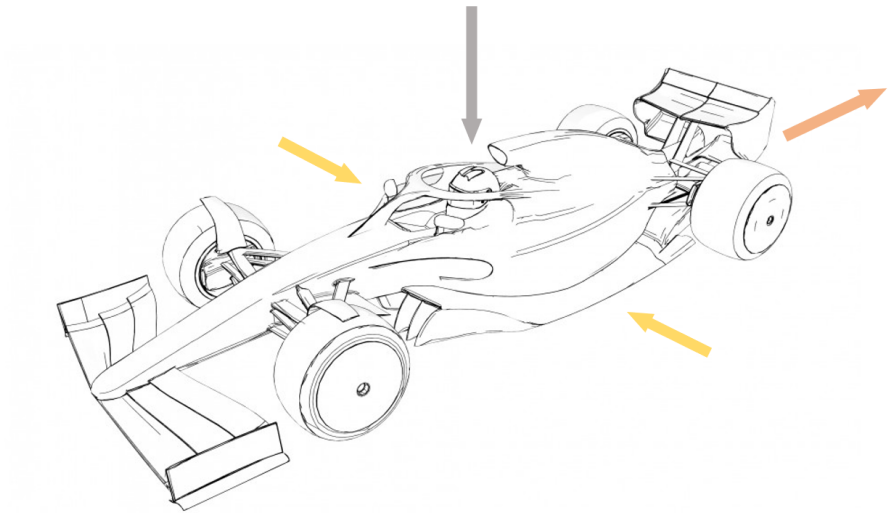

Figure 2.2: Forces acting on a F1 car in a racing situation.

The majority of the downforce generated by the car comes from the floor, but there are also big contributions from the front and rear wings. Aerodynamicists seek to get them all working in harmony to deliver maximum car performance. A description the shape and function of each of the elements studied in this project is presented as follows.

2.1 Underfloor

From 1983, when ground effect aerodynamics was banned by the FIA, the regulations required the underfloor to be a flat surface, with the diffuser section at the rear offering the ability to add vertical volume. With the new rules introduced in 2022, the underfloor took on a much more in-depth design scheme. Greater variation in its geometry and overall shape of the floor were allowed. A comparison between the underfloors used until 2021 and the ones used from 2022 is depicted in Figure 2.3.

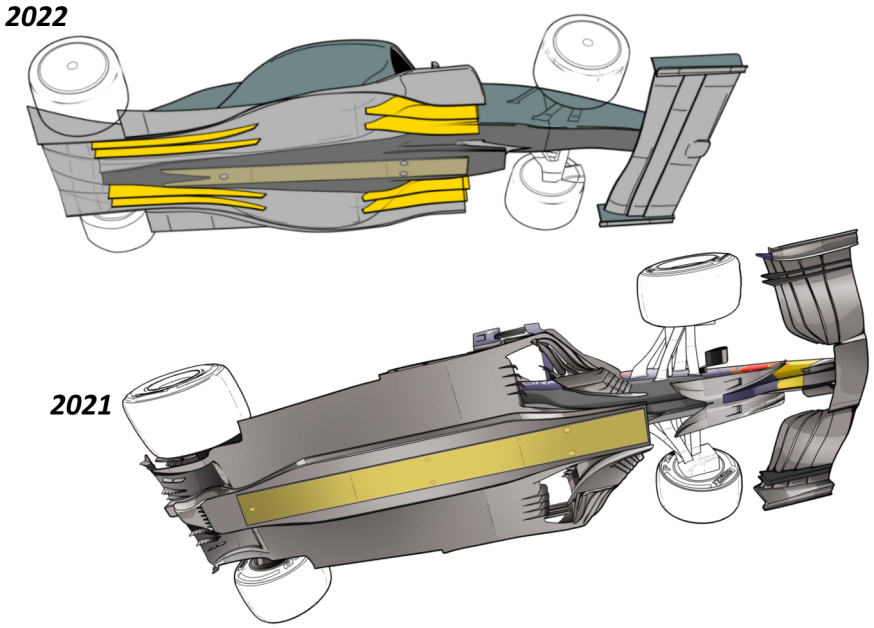

Figure 2.3: Comparison between the 2021 and 2022 underfloors. [2]

There are many different airflows beneath the floor, and the key is in controlling them and getting them to work together.

Starting from the leading edge of the underfoor, it can be seen that several internal vertical turning vanes have been included, with the aim of controlling better the turbulence coming from from another car. Continuing downstream, the underfloor profile changes its shape in order to establish two distinct Venturi tunnels, changing its height to form diffusers. These diffusers will provoke the expansion of the airflow passing under the vehicle, increasing its speed and creating a low pressure zone, following Bernoulli's principle. A sketch of the underfloor designed by *Scuderia Ferrari* for its 2023 car is presented in Figure 2.4.

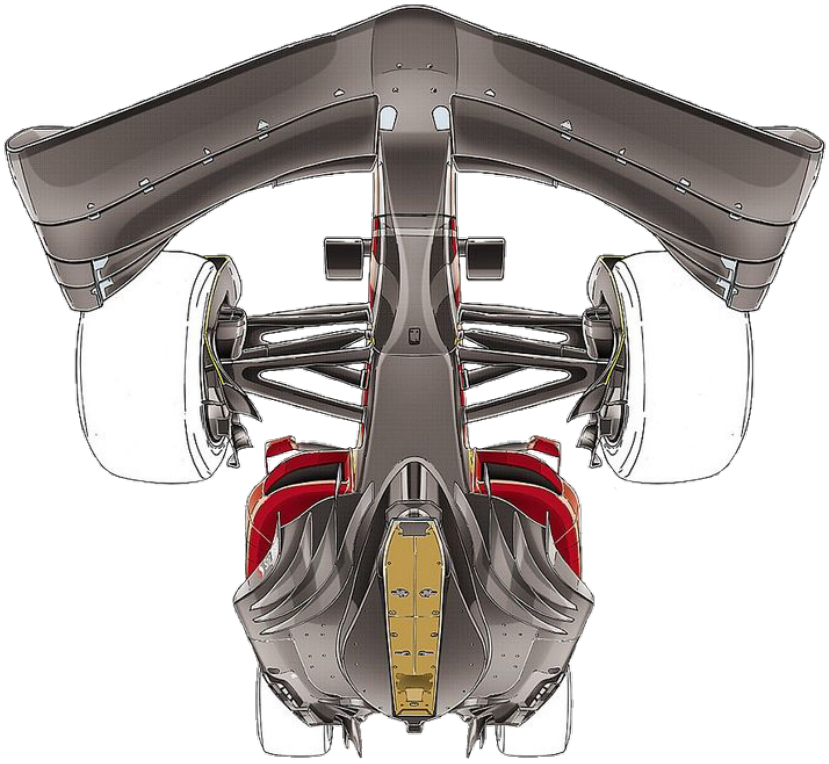

Figure 2.4: *Ferrari SF23* underfloor design for the 2023 season. [3]

2.2 Beam wing

The beam wing is another of the elements introduced by the 2022 regulations, after being banned since 2014. This is an element joined to the lower zone of the rear wing's endplates, close to the vehicle's exhaust pipe, as Figure 2.5 shows. It works as a prolongation of the diffusers located in the underfloor. Its function is to allow a better and smoother expansion of the airfow at its exit from the diffusers. In this way, the beam wing works jointly with the underfloor to provide a rapid evacuation of the airflow and enhance the downforce created by the underfloor.

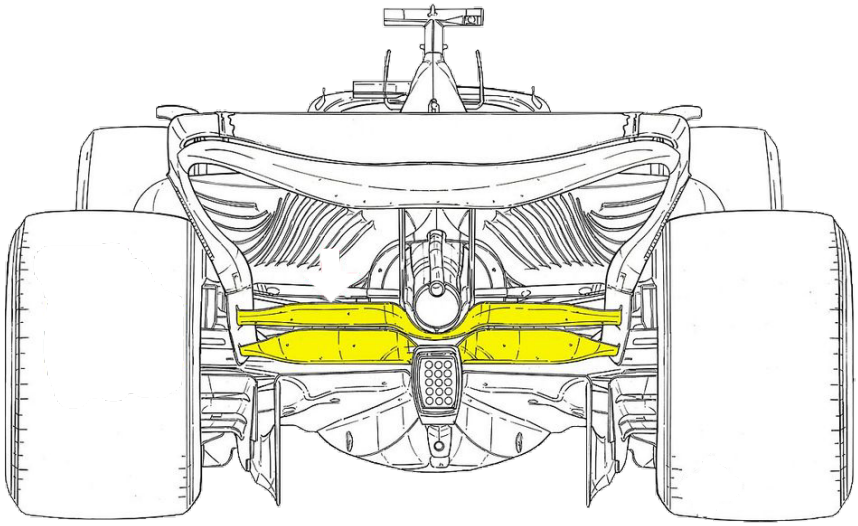

Figure 2.5: Beam wing representation in a standard 2023 F1 car, highlighted in yellow. [4]

2.3 Rear wing

The rear wing introduced by the 2022 regulations has two main functions. One of them is creating downforce. The other one is directing the turbulent wake generated by the car high into the air, away from the front wing of the car that comes behind. In this way, the following car receives a less disturbed air to contend with when setting up an overtake to the leading car (the aerodynamic surfaces work less efficiently if the incoming air is turbulent, making the car generate less downforce).

This new design of rear wing was conceived as a continuous shape, avoiding sharp edges and radiusing the corners of the endplates. This reduces the effectiveness of the rear wing's elements in generating downforce, since maximum possible pressure difference between the underside and upper surface (necessary to maximize downforce) is not achieved. Nevertheless, this configuration of rear wing greatly reduces the turbulent vortices that spill off the wing corners, where separate airflows mix. As well, the endplates sweep inwards, narrowing the aerodynamic wake of the car and preventing it from spilling outwards to the detriment of the car that goes behind. An example of this rear wing geometry is presented in Figure 2.6.

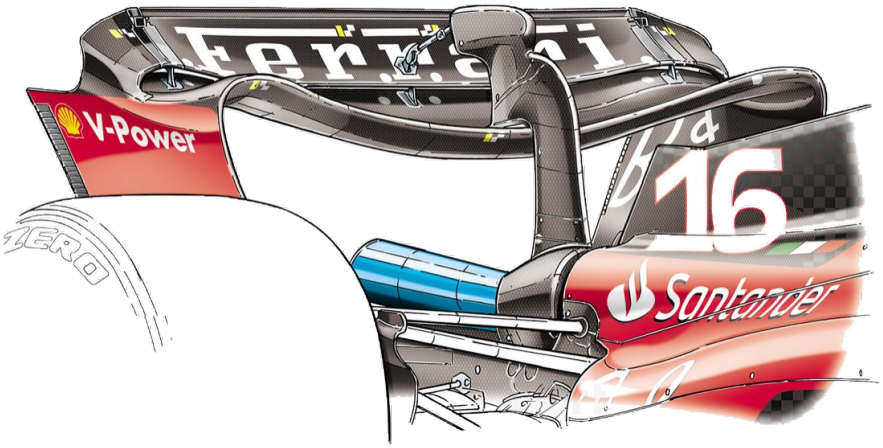

Figure 2.6: *Ferrari SF23* rear wing for the 2023 season. [5]

2.4 DRS system

The DRS (*Drag Reduction System*) is a bodywork integrated in the rear wing of F1 cars, which was introduced in the 2011 campaign and remains in use after the new rules reset of the 2022 season.

This device is basically a flap which can move in response to the driver's commands, allowing the opening or closing of a slot in the rear wing of the vehicle. It can only be activated under certain racing conditions established by the rules and in specific zones of the circuit. Figure 2.7 shows the DRS system when it is closed and when it is open.

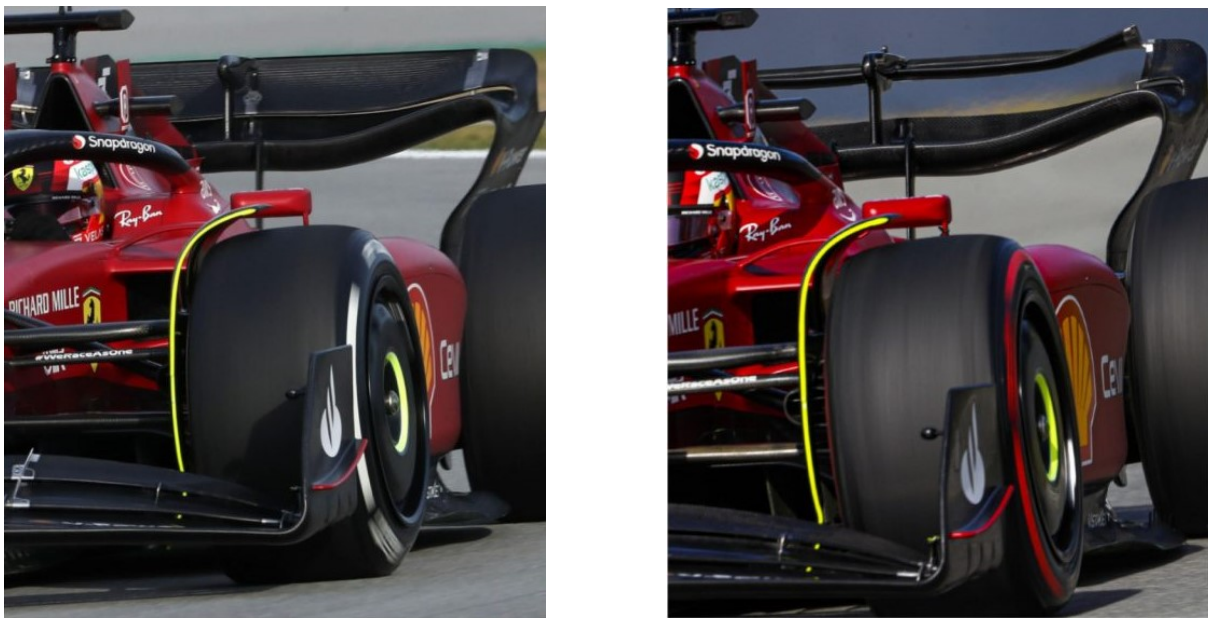

(a) DRS closed. (b) DRS open.

Figure 2.7: *Ferrari F175* rear wing, incorporating the DRS system. [6]

As its name suggests, the function of the DRS is reducing the aerodynamic drag of the vehicle. When the driver activates the system, the flap turns upwards, reducing its angle with respect to the airflow incidence. In this way, the frontal area of the car's rear wing becomes smaller, letting the air flow through the opening that is formed and thus reducing drag.

This variation in the rear wing's geometry also leads to a reduction in the generated downforce. When the DRS is not active, the reversed airfoil shape of the rear wing originates a suction in its underside and a pressure increase in its upper side, leading to a vertical force directed downwards (downforce). When the DRS is activated, given that the flap adopts an almost horizontal position, the pressure gradient between its underside and upper side diminishes, reducing the magnitude of the downforce.

Consequently, the DRS system is useful in situations when high speeds and are needed rather than downforce. This is the case of straights, where there are no significant lateral forces, so less downforce allows faster acceleration and potential top speed. This is the reason why the DRS is specially conceived for overtaking.

It can be concluded that the underfloor, beam wing and rear wing operate all together and complement. First, the air exiting the Venturi channels of the underfloor follows the angle of the underside of the beam wing, and then meets the flow that has been funnelled by the

endplates. The whole air convergence is then thrown upwards away from the next car. In this way, the desired levels of downforce are produced, the airflow is directed away from the next car and the turbulent wake downstream the vehicle is reduced as much as possible.

3 Design of the aerodynamic elements

For the development of this project, a real underfloor, beam wing and rear wing are considered to study their aerodynamic function and behaviour. These elements correspond to a vehicle currently competing in the Formula 1 2023 championship, the *Ferrari SF23*. Hence, they have been designed according to the new regulations introduced by the FIA in the 2022 season.

The *Ferrari SF23* model is shown in Figure 3.1

Figure 3.1: *Ferrari SF23*. [7]

Given that this is Scuderia Ferrari's current car to compete in the F1 championship, detailed dimensions and plans of the car are not available and remain protected by the team. Consequently, an approximated recreation of the elements analysed in this project has been carried out. For doing so, the computer-aided design software *Autodesk Fusion 360* has been employed. In the following subsections, the CAD model of each of these elements is presented.

3.1 Underfloor

The underfloor is made up of a set of surfaces with complex shapes that fulfill certain functions, as commented in subsection 2.1.

It is divided into two channels separated by a flat surface whose width gets smaller as the rear end of the underfloor is reached, known as the keel.

At the leading region of the underfloor, six turning vanes (three in each channel) are placed. Then, the underfloor profile changes its shape gradually, forming Venturi tunnels that act as diffusers. These diffusers allow the expansion of the airflow passing under the vehicle, increasing its speed and creating a low pressure zone.

3.1.1 CAD model

Figure 3.2: Isometric view of the underfloor model, seen from below.

Figure 3.3: Isometric view of the underfloor model, seen from above.

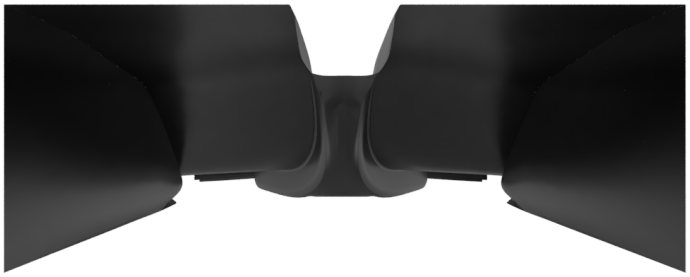

Figure 3.4: Rear view of the underfloor model, showing the diffuser exit.

3.1.2 Main dimensions

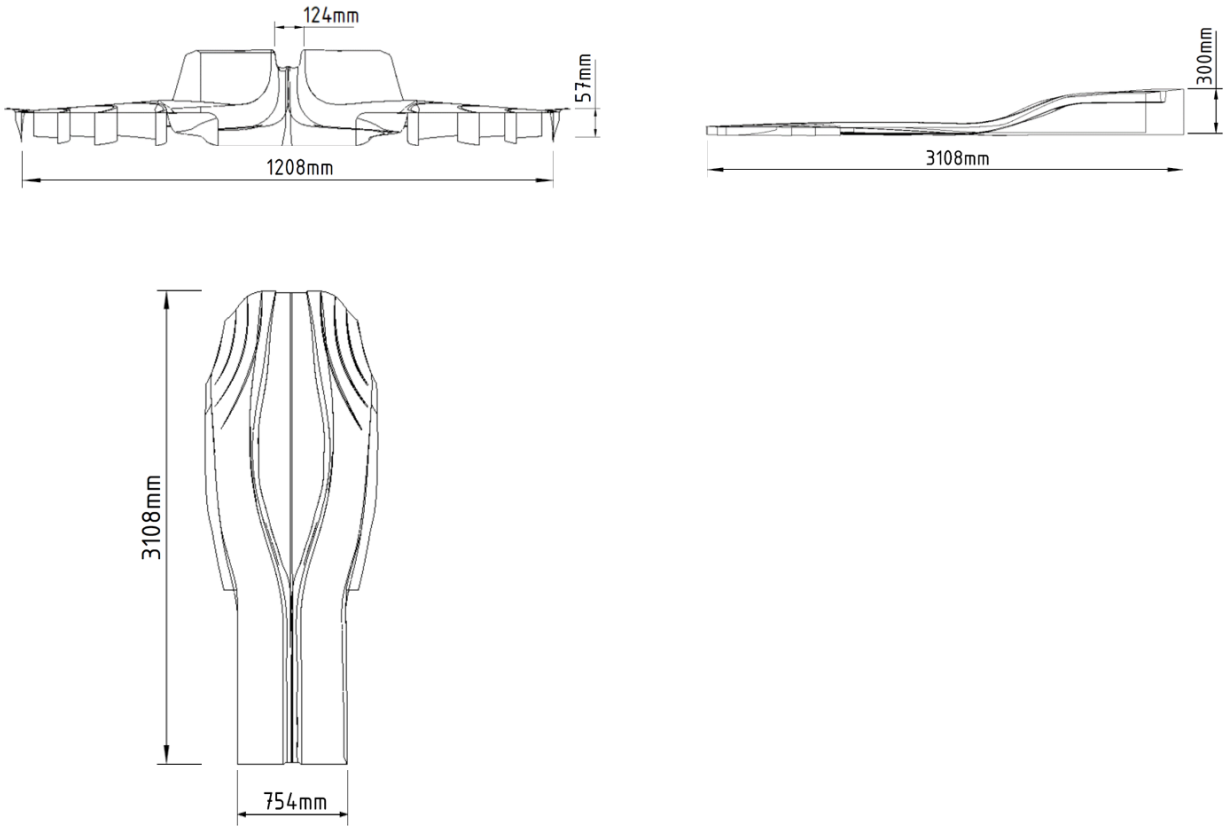

Figure 3.5: Main dimensions of the underfloor.

3.2 Beam wing

3.2.1 CAD model

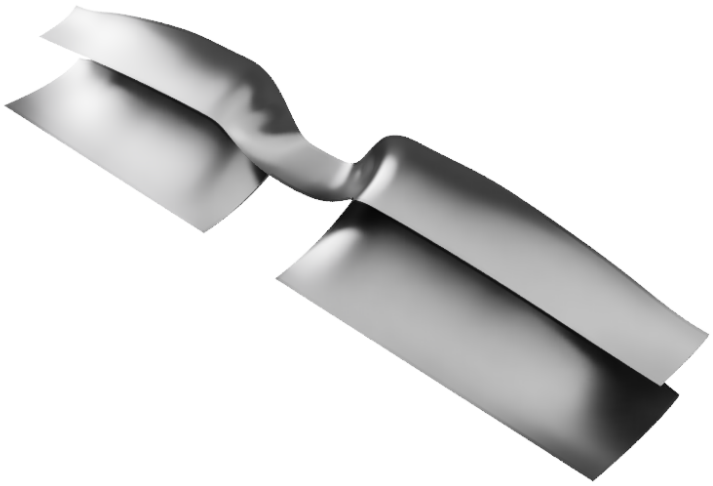

Figure 3.6: Isometric view of the beam wing model.

3.2.2 Main dimensions

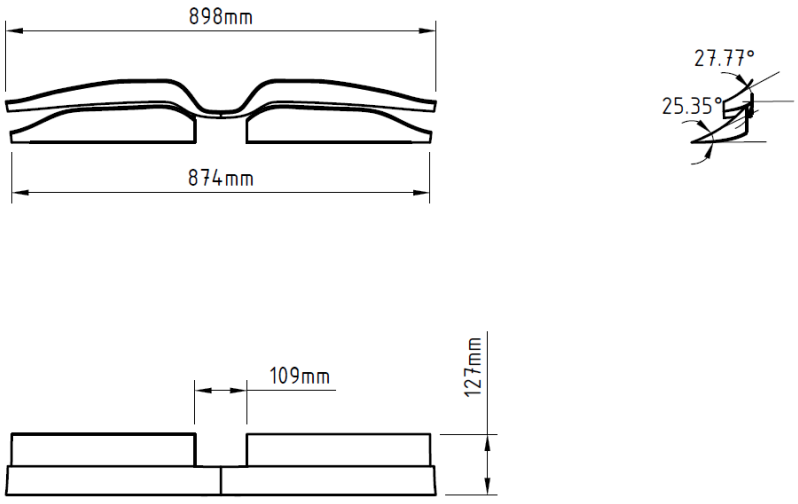

Figure 3.7: Main dimensions of the beam wing.

3.3 Rear wing

3.3.1 CAD model

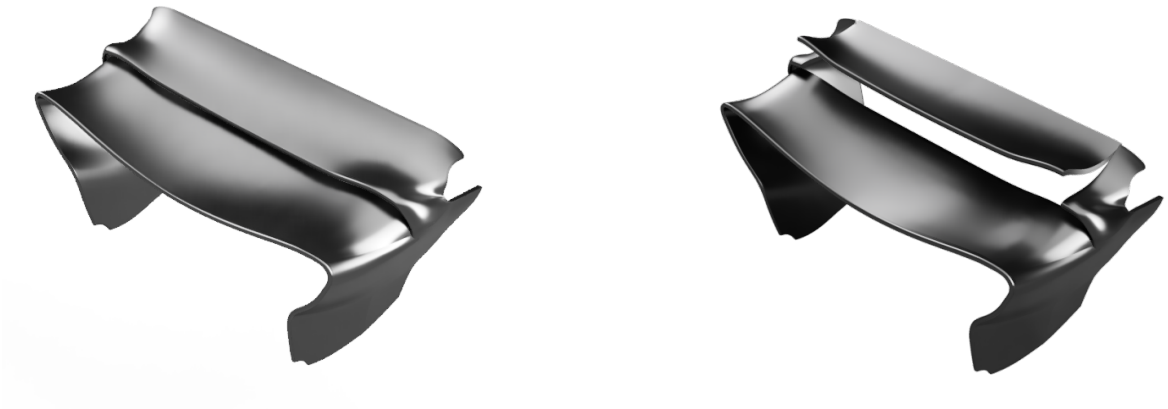

(a) DRS closed. (b) DRS open.

Figure 3.8: Isometric view of the rear wing model.

3.3.2 Main dimensions

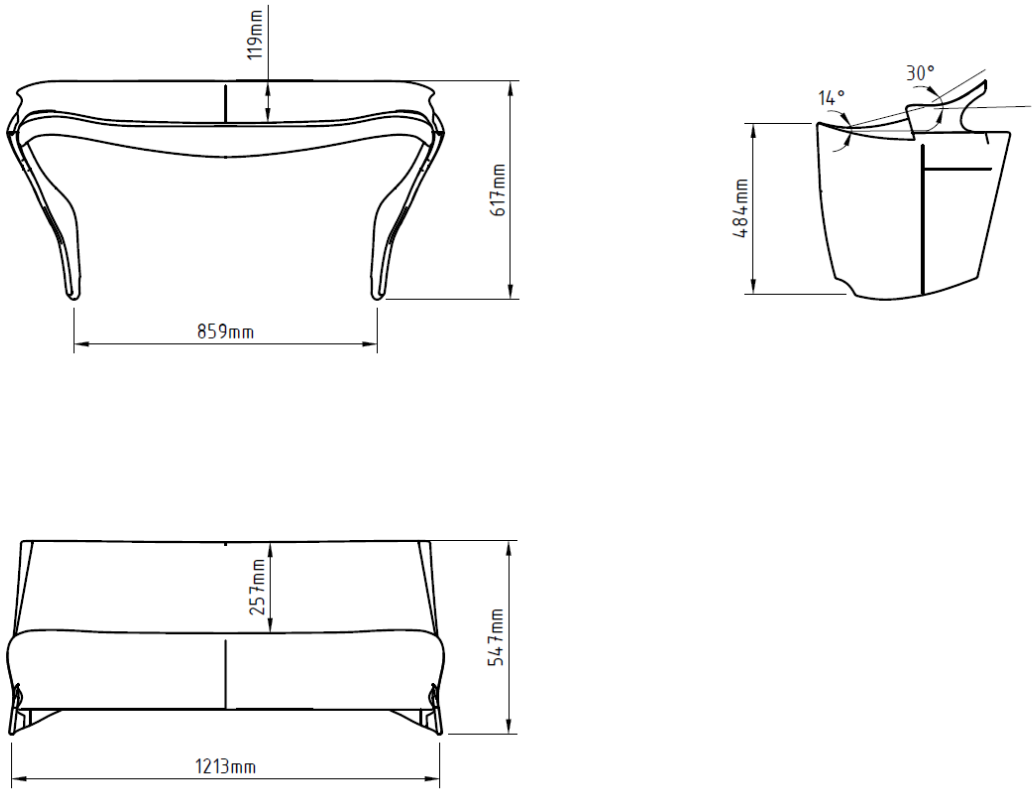

Figure 3.9: Main dimensions of the rear wing.

3.4 Whole assembly

The whole assembly integrating the underfloor, beam wing and rear wing is shown in Figure 3.10, Figure 3.11 and Figure 3.12.

Figure 3.10: Isometric view of the whole assembly model.

Figure 3.11: Lateral view of the whole assembly model.

(a) Frontal view.

(b) Rear view.

Figure 3.12: Frontal and rear views of the whole assembly model.

4 Implementation in CFD software

The aerodynamic analysis of the elements described previously is done by means of *Simcenter STAR-CCM+*. This is a commercial Computational Fluid Dynamics (CFD) based simulation software, developed by the german multinational *Siemens*. The process comprises a series of steps, which are detailed in the incoming subsections.

4.1 CAD model importation

The model created in *Autodesk Fusion 360* is saved in .step format, a data exchange form used for representing 3D objects in CAD. Then, it is imported as a Surface Mesh in *STAR-CCM+*.

4.2 Geometry

Two parts are established for the geometry: the imported CAD model and a domain. The domain is created as a block part, and its function is to recreate the environment that surrounds the Formula 1 car in a real racing situation. A scene of the studied elements of the vehicle inside the domain is shown in Figure 4.1.

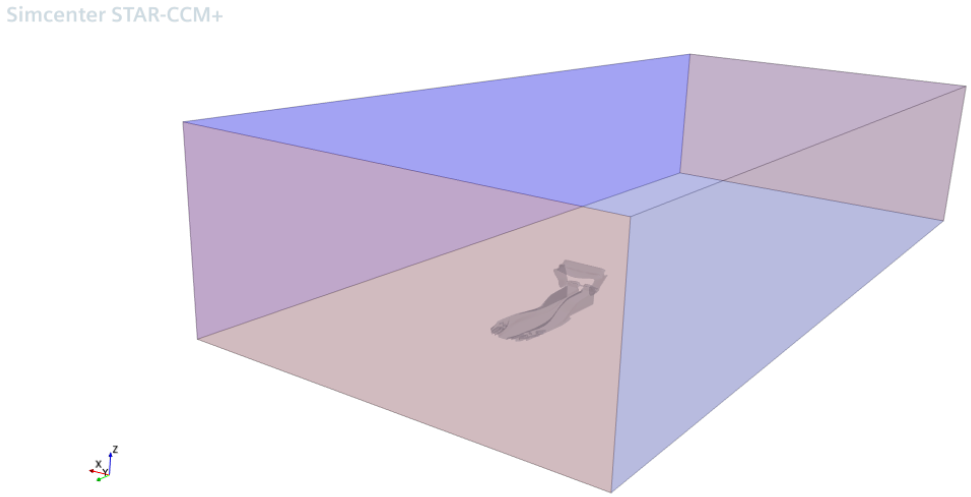

Figure 4.1: Imported CAD geometry inside the domain.

4.3 Regions

A region is assigned to each of the surfaces of the parts. All the surfaces that compose the CAD model are combined, forming one single surface of the CAD model. Then, several boundary conditions are established, each one corresponding to a surface of the CAD and domain set. These boundary conditions and their type are listed below:

- CAD model: wall
- Inlet: velocity inlet
    * Velocity: 60 m/s, normal to boundary
    * Turbulent viscosity ratio: 10
- Outlet: pressure outlet
    * Pressure: 0 Pa
    * Turbulent intensity: 0.01
    * Turbulent velocity scale: 1 m/s
- Track: wall
- Surroundings: symmetry

The wall boundary is a solid boundary, which does not allow flow propagation through it and will reflect waves back off itself. Then, the inlet allows flow to enter the established domain. The magnitude and direction of the flow's velocity entering the domain are determined. As for the outlet, it is where the flow comes out of the control volume. The pressure at this outlet is specified as well. Finally, the symmetry plane boundary allows to reduce the computational effort and resources modelling only a portion of the complete geometry by applying symmetry boundary conditions. All these boundaries are presented in Figure 4.2.

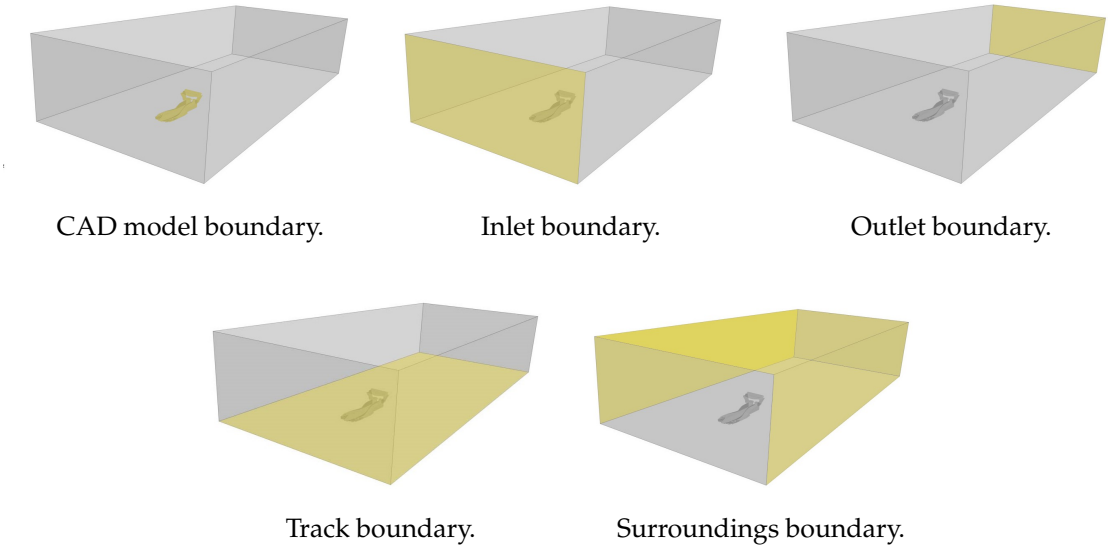

CAD model boundary. Inlet boundary. Outlet boundary.

Track boundary. Surroundings boundary.

Figure 4.2: Boundaries of the domain and CAD model.

4.4 Physical models

It is necessary to determine a series of physical models that can characterize the flow and its nature. In that way, the computations of the software become more realistic and adapted to the real situation that aims to be modelled.

In this case, the studied flow is involved in a racing situation. It is assumed that the car is competing in a circuit located at sea level, with standard temperature and pressure conditions (288.15 K and 101.325 kPa, respectively). Taking this into account, the selected physical models are:

- Three-dimensional model: designed to work on three-dimensional meshes in cases where all spatial directions are relevant.
- Implicit unsteady time: the flow is defined as unsteady, provided that the flow conditions in the situation studied in this project vary in space and time. The unsteady analysis provides a more accurate approach of the car's aerodynamic performance, since the flow phenomena that take place around the car (such as vortices or flow separation regions) evolve over time until the flow stabilizes. It is necessary to determine an implicit unsteady time-step during which the temporal resolution of the simulation is carried out. During each time step, the equations characterizing the flow are recalculated to obtain

new solutions for the flow variables at that particular time instant. Then, once the solution has converged for a given time step, the simulation time is advanced to the next time step. In this way, the simulation progresses by updating iteratively the solution from one time step to the next one.

- Segregated flow: the segregated solver splits the problem up into two or more segregated steps. These individual segregated steps are smaller than the full system of equations that is solved with the fully coupled approach. This means that the software does not solve for all of the unknowns at one time, but instead solves sequentially within a single iteration, and thus less memory is required.

- Gas: the fluid interacting with the car is air, which is a gas.

- Ideal gas: an ideal gas is essentially a theoretical composition of point masses moving in random motion, that are not subject to interparticle interaction. Considering standard temperature and pressure conditions at the circuit, then it can be assumed that the behaviour of the ambient air that surrounds the F1 vehicle approaches that of an ideal gas.

- Isothermal fluid: the air is assumed to remain isothermal in its interaction with the car, meaning that its temperature keeps a constant value no matter the variations that it may undergo in other properties. Thermal effects are indeed important in Formula 1. However, these have to do with the generation of heat by elements like the power unit, exhaust system or brakes, rather than as a consequence of aerodynamic effects. In the case of this study, given that only a partial analysis of the car's aerodynamic surfaces is carried out, the possible thermal variations of the airflow due to the presence of the components named previously are not considered.

- Turbulent: turbulent flow is characterized by irregular variations of fluid particles, undergoing velocity changes in both magnitude and direction. For the development of this project, turbulent flow is assumed. The airflow meets the car being laminar, considering a situation in which no other vehicles are ahead of the studied car. Then, a part of this clean air passes through the underfloor and another part passes through the rear wing. During its interaction with these elements, the flow experiences unsteadiness, vorticity and three-dimensional effects. Consequently, it is necessary to consider the turbulent flow model.

- K-Epsilon Turbulence: this is the most common model to simulate the mean flow characteristics for turbulent flow conditions, like the ones that characterize the situation studied. It belongs to the Reynolds-averaged Navier Stokes (RANS) family of turbulence models, where all the effects of turbulence are modeled. K-Epsilon is a two-equation model. This means that, in addition to the conservation equations, it includes two extra

transport equations (turbulent kinetic energy and turbulent dissipation) to represent the turbulent properties of the flow.

4.5 Initial conditions

For the *STAR-CCM+* solver to provide a solution for the conservation and transport equations, some initial conditions of the flow must be defined. These are listed below:

- Reference pressure: 101325 Pa
- Velocity: 0 m/s

4.6 Derived parts

Derived parts are useful for studying the flow behaviour in a specific region of interest. To perform the aerodynamic analysis pursued in this project, three derived parts are employed:

- Plane section
- Resampled volume
- Streamline

4.7 Previous considerations

Some important aspects related to the aerodynamic study and to the assumptions taken in the *STAR-CCM+* analysis are briefly commented in the lines that follow.

4.7.1 Studied forces

As commented in section 2, there are three basic forces acting on F1 cars: downforce, drag and lateral forces. In this project, a scenario where the car races in a straight is assumed. Hence, lateral forces, which are mostly a consequence of the centrifugal force generated when the car goes through a corner, are neglected. Only downforce and drag will be studied.

4.7.2 Neglected flow phenomena

It is important to mention that the aerodynamic phenomena that take place on top of the underfloor, before reaching the rear wing of the car, are neglected. This project consists of a partial study of a Formula 1 car, focusing on the aerodynamic components on the rear half of the vehicle and on the downwash behaviour of the flow. The structure of the car that should be present on top of the underfloor is not analysed.

4.7.3 Unsteadiness

As explained in subsection 4.4, an unsteady situation is considered (for both cases), with an associated time step. This time step takes a value of 0.05 s. As well, a maximum physical time of 10 seconds is established for the CFD simulation. This means that the flow behaviour is solved for a situation in which the F1 car is racing during a period of 10 seconds, performing a certain number of iterations (set to 5) for each time step of 0.05 seconds.

4.7.4 Domain size

A [10 x 22 x 4.526] m domain is created, with the imported CAD model inside. These dimensions are established big enough to cover the area of influence of the car, so as not to miss any relevant information about the flow's behaviour.

4.7.5 Derived parts employed for showing results

As for the pressure, velocity magnitude and turbulent viscosity rate, they are measured at a plane section located at **x =** 0.15 m, normal to the XZ plane. This section has been chosen because it is not interrupted by the surfaces of the underfloor, so it offers a clean view of the devices that aim to be analysed. Then, vorticity is measured in a resampled volume that contains the aerodynamic elements studied in the project, given that it adapts better to the three-dimensional nature of this magnitude. Finally, a streamlines stream is employed for representing the streamlines scene.

4.7.6 Bernoulli's principle

The effects that the aerodynamic elements studied in this project provoke on the flow's behaviour can be explained with Bernoulli's principle.

This statement derives from the principle of conservation of energy. It establishes that, for an ideal fluid (this is, incompressible, non-viscous and laminar), the sum of the pressure, kinetic and potential energies per unit volume remains constant at all points:

$$p + \frac{1}{2} \cdot \rho \cdot v^2 + \rho \cdot g \cdot h = \text{ constant}$$

In this case, the geometry in which Bernoulli's principle takes place is the volume between the F1 car's underfloor and the track. Since this region is always horizontal (with no height differences), the acceleration of the fluid due to gravity can be neglected. This leads to:

$$p + \frac{1}{2} \cdot \rho \cdot v^2 = \text{ constant}$$

The relation that pressure and velocity hold in order to fulfill this principle is analysed in the next sections.

4.7.7 Studied cases

Two cases are studied: a high-downforce case and a low-drag case. In both cases, it is assumed that the car starts is stopped (due to the initial condition of 0 m/s velocity) and accelerates till reaching 60 m/s (inlet boundary condition) in a straight, facing clean and laminar air. Nonetheless, the first case simulates a situation in which the DRS system is closed, while the second one simulates a scenario in which the DRS has been activated. This implies a variation in geometry that changes the flow's behaviour.

5 High - downforce case

5.1 Meshing

Regarding meshing, it can be defined as a discretized representation of the computational domain, which the physics solvers use to provide a numerical solution. It represents one of the main steps of the analysis, given that it determines the computational cost of the simulation, as well as its accuracy and convergence rate.

5.1.1 Models

The meshing models chosen for this analysis are the following:

- Polyhedral mesher: it generates a mesh made up of polyhedral-shaped cells. It is a good balance between speed and efficiency, and creates a high-quality mesh.
- Surface remesher: this tool remeshes the model and resolves face quality and face proximity errors. In this case, given the 3D model and domain, this function is necessary for ensuring a consistent mesh across all parts.
- Surface wrapper: it is a function that wraps the geometry of interest to create a volume that does not contain intersecting surfaces or sharp edges. Its use is recommended when the input geometry to study has a high level of detail, like the case of this analysis.

5.1.2 Reference values

The main parameters defining the mesh are the following:

- Base Size: 0.06 m
- Surface Growth Rate: 1.3
- Relative Minimum Size: 25
- Relative Target Size: 100

5.1.3 Diagnostics

- Cells: 3926983

- Faces: 28225460
- Verts: 24527762

An image of the resulting mesh is depicted in Figure 5.1.

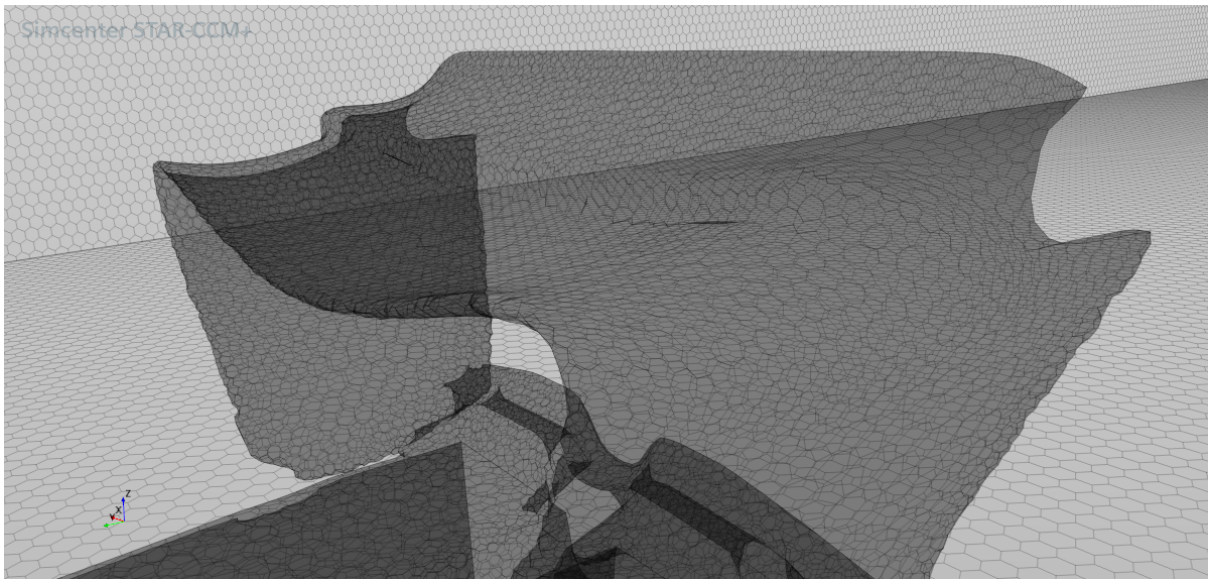

Figure 5.1: Mesh detail of the high-downforce case geometry.

5.2 Analysis of residuals

Most of the fluid flow situations analysed in CFD software like *STAR-CCM+* are non-linear, which means the change of the output is not proportional to variations in the input. Hence, the conservation and transport equations cannot be solved as a system of linear equations. Instead, the studied geometry is discretized into a large number of smaller of control volumes, and an iterative process is followed to successively improve a solution in each of these volumes until convergence is reached.

The most common method for assessing the convergence of the iterative process is the analysis of residuals. The residual is a measure of the difference between the predicted value of a certain variable and the actual calculated value. So it directly quantifies the error in the solution of the system of equations. Hence, every small control volume has its own residual value for each of the equations being solved. The residuals of these equations should converge as close to zero as possible so as to obtain numerically accurate solutions.

In the case of an unsteady case like this one, a certain number of iterations is performed during each time step. In each iteration, the discretized equations are solved to update the solution of the flow variables for that particular time step. After completing that number of iterations, the solution is assessed to determine if it has converged or reached an acceptable level of accuracy. In case of not converging, additional iterations may be performed until convergence is achieved. Once the solution for the current time step has converged, the simulation proceeds to the next time step, and the process is repeated. This process is what defines the fluctuating shape of the residuals in unsteady simulations.

The solver of *STAR-CCM+* performs iterative calculations for the following equations: continuity, energy, Tdr (turbulent dissipation rate), Tke (turbulent kinetic energy), momentum in X, momentum in Y and momentum in Z.

Provided that the car is racing during a period of 10 seconds and 5 iterations are performed for each time step of 0.05 seconds, a total of 1000 iterations are performed by the solver. Figure 5.2 plots the evolution of the conservation and transport equations's residuals for this number of iterations.

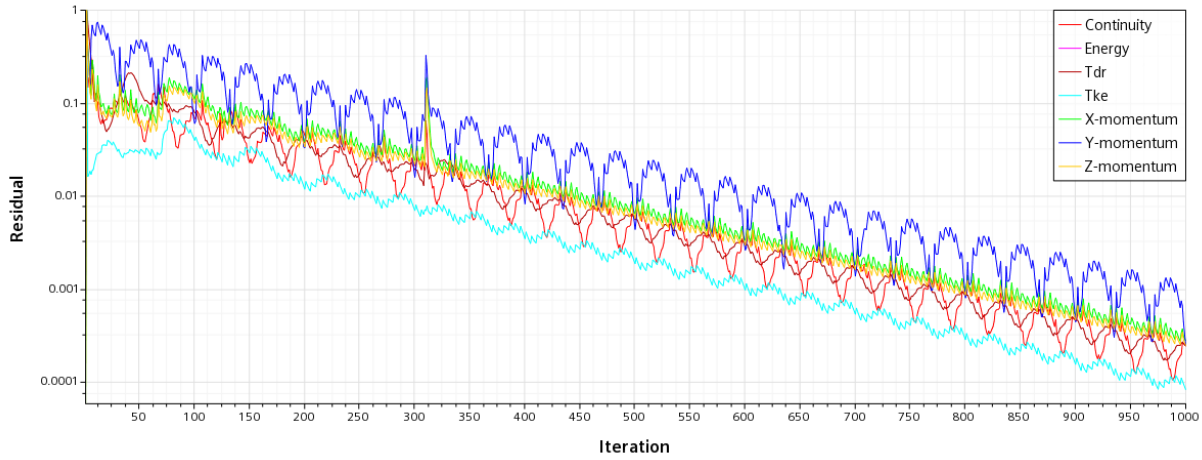

Figure 5.2: Residuals plot for the high-downforce case.

After 10 seconds of simulation, it is obtained that the residuals of continuity, x-momentum, y-momentum, z-momentum and tdr are of the order of 10^{-4}. Residuals of tke are of the order of 10^{-5}, and residuals of energy are null, given that the flow is asssumed to be isothermal (as commented in subsection 4.4), so there are no thermal energy variations. These are values that remain within 10^{-3} and 10^{-6}, which is commonly considered an acceptable interval of residuals for obtaining stable solutions. This means that, after 10 seconds, the flow around the car has already reached a stable behaviour.

5.3 Results

5.3.1 Velocity

Figure 5.3, Figure 5.4 and Figure 5.5 show the velocity contours of the airflow when it encounters the F1 car, at several different time instants.

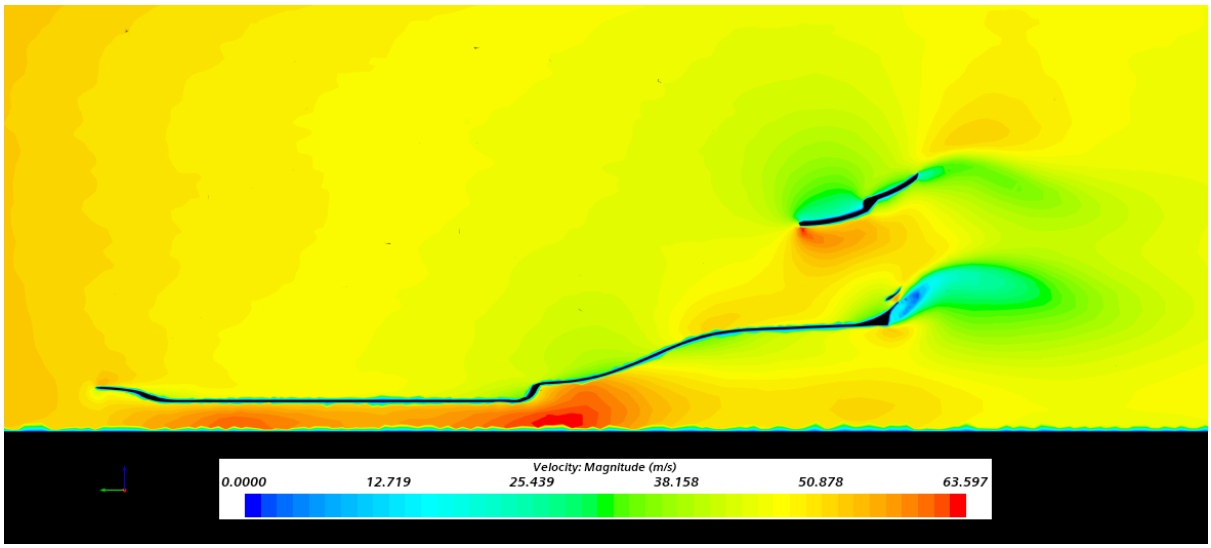

Figure 5.3: Velocity magnitude contours of the whole assembly (0.1 s).

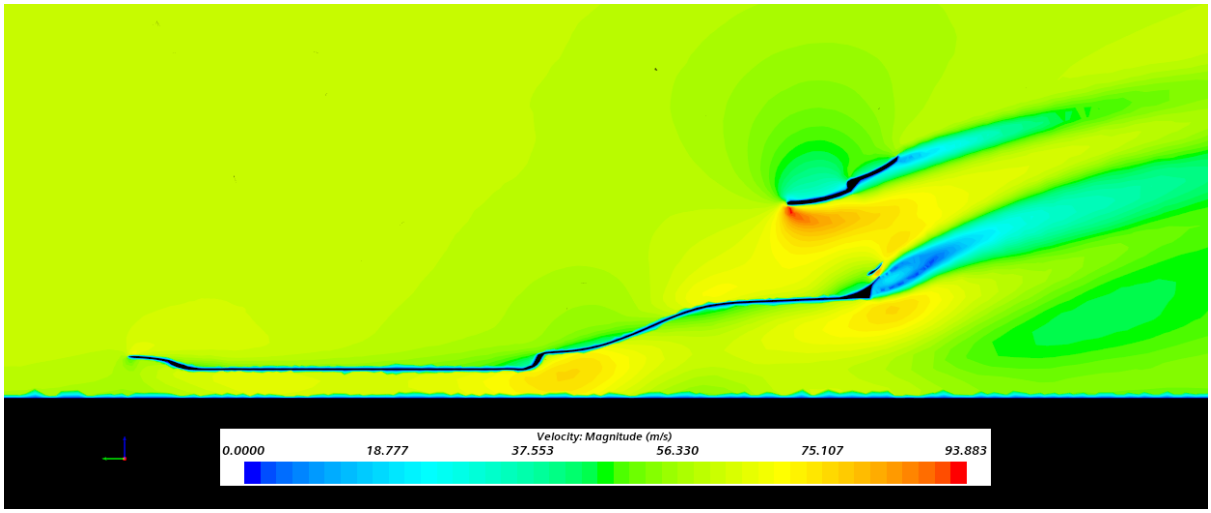

Figure 5.4: Velocity magnitude contours of the whole assembly (2.5 s).

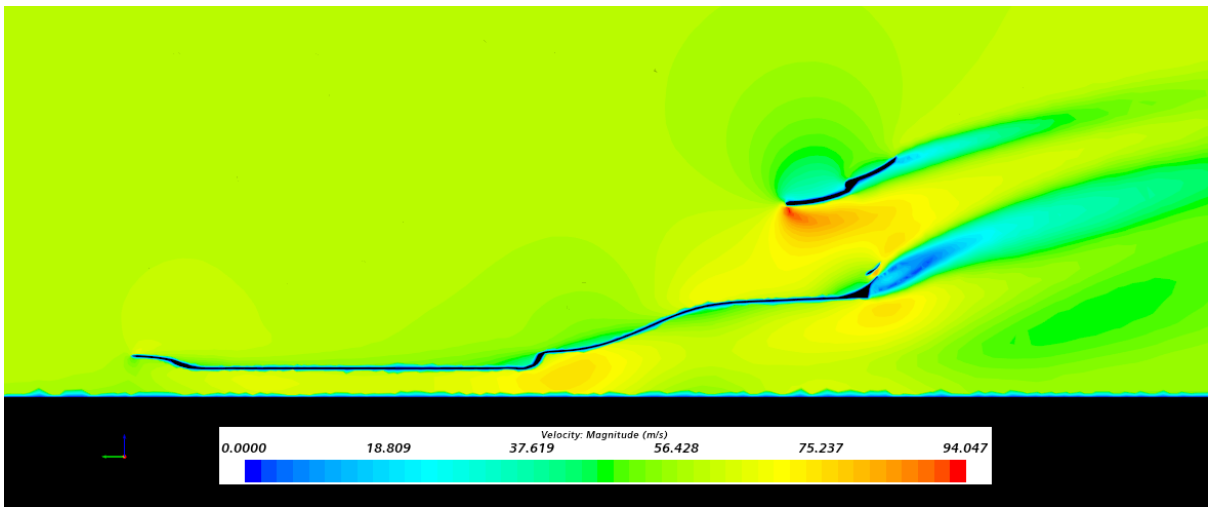

Figure 5.5: Velocity magnitude contours of the whole assembly (5 s).

It can be observed how the flow has not reached yet the 60 m/s inlet velocity when 0.1 seconds have passed. During the first seconds, it keeps developing and setting up.

Now, the velocity field at 10 seconds is analysed in Figure 5.6, when the flow is already stabilised around the car. It can be observed that the air approaches the front of the underfloor at 60 m/s, which is the condition established for the velocity inlet. Once it reaches the underfloor, its velocity slightly decreases due to the presence of a body that interrupts the flow.

As for the air that flows between the underfloor and the ground, several phases can be distinguished. From the beginning of the underfloor till the beginning of the diffuser (where the underfloor curves upwards), the reduction of volume leads to an increase in the flow's velocity along the Venturi channels, up to values around 75 m/s. Then, the underfloor's volume increases gradually, acting as a diffuser. Here, the flow gradually decelerates to reach its initial value. Finally, it exits the underfloor and adopts the initial velocity it had before entering it.

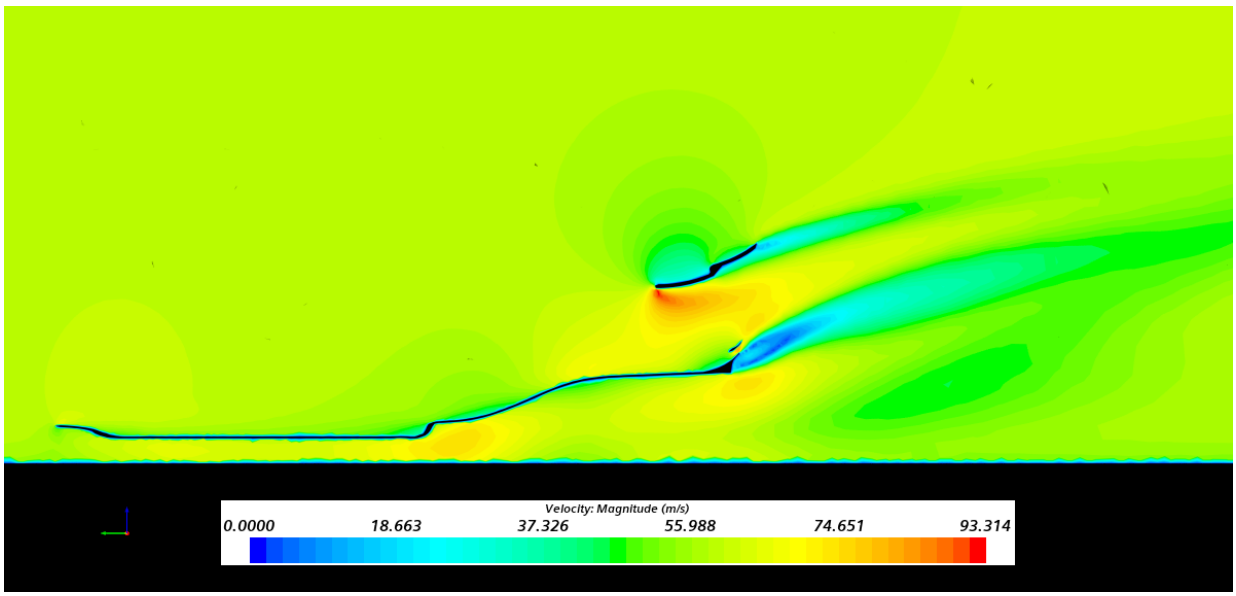

Figure 5.6: Velocity magnitude contours of the whole assembly (10 s).

As for the flow that meets the rear wing of the car, the reversed airfoil shape of this element leads to variations in velocity. On the one hand, the flow passing under this surface experiences a velocity increase due to the local expansion that this element provokes in the fluid. On the other hand, the flow passing over the surface is forced to a compression that leads to a velocity decrease.

Figure 5.7 shows a detailed view of the flow when it encounters the rear wing and the beam wing. It can be observed that the presence of these surfaces interrupts the path followed by the air, leading to reversed flow and a decrease in velocity downstream of these elements, down to values between around 0 m/s and 35 m/s.

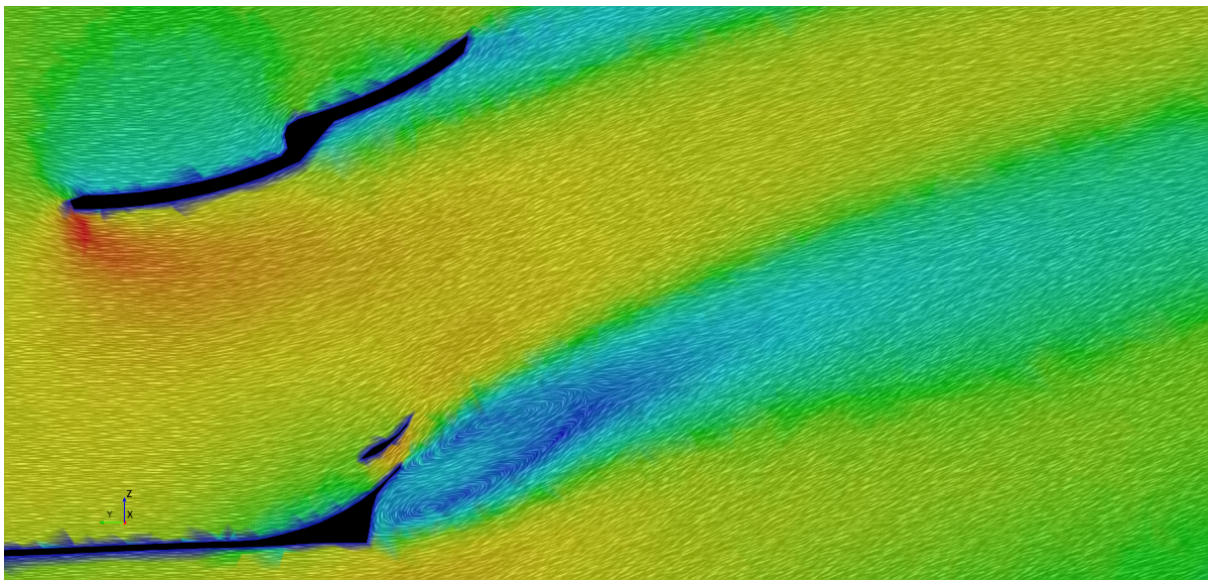

Figure 5.7: Detail of the velocity magnitude and direction of the flow downstream the rear wing and beam wing (10 s).

5.3.2 Pressure

Figure 5.8, Figure 5.9 and Figure 5.10 represent the pressure distribution around the aerodynamic elements at different instants when the flow is not still completely developed:

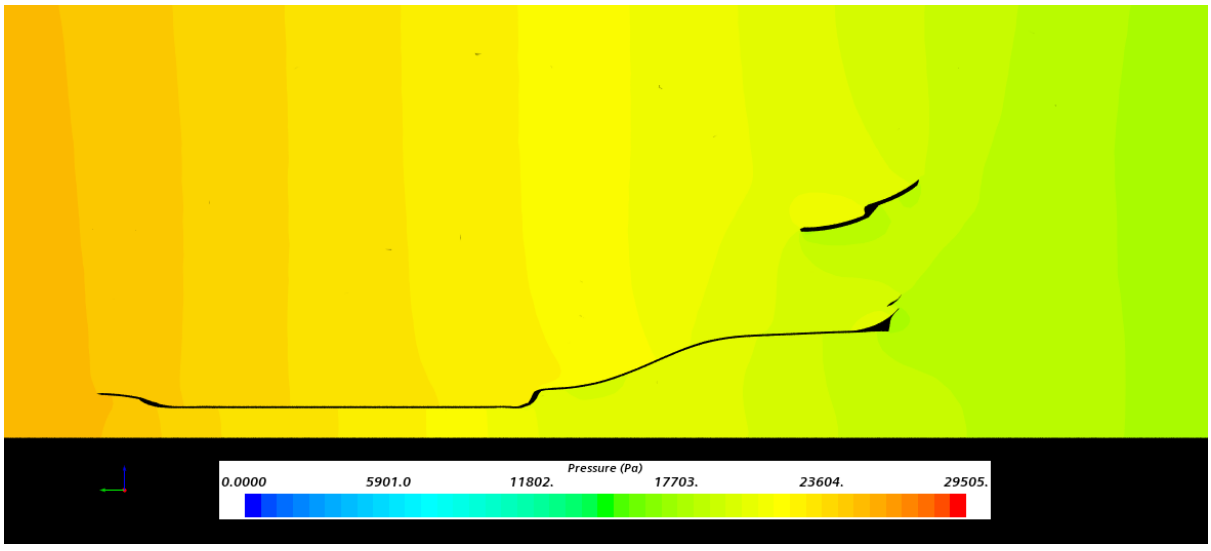

Figure 5.8: Pressure contours of the whole assembly (0.1 s).

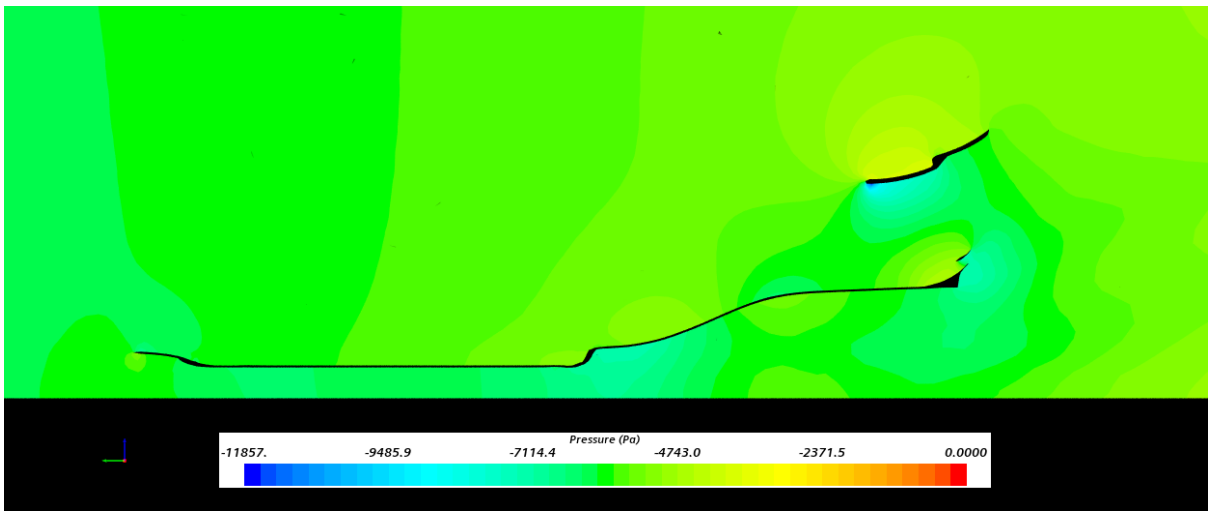

Figure 5.9: Pressure contours of the whole assembly (2.5 s).

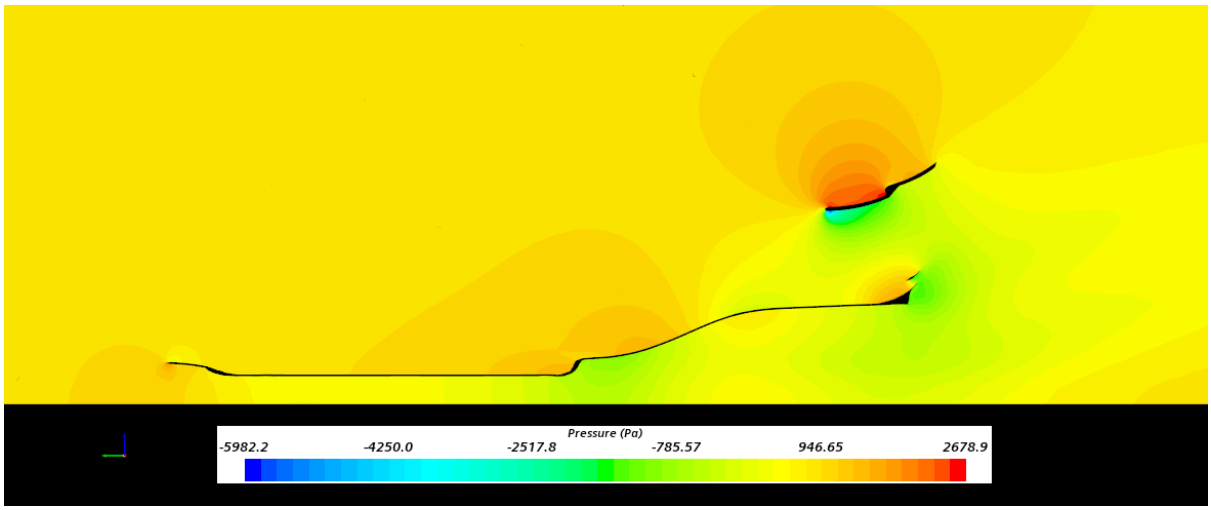

Figure 5.10: Pressure contours of the whole assembly (5 s).

Figure 5.11 depicts the pressure contours of the stabilised airflow after 10 seconds have passed.

Before reaching the aerodynamic surfaces of the car, the pressure takes a value of 0 Pa. This value is actually equivalent to the atmospheric pressure set as reference (101325 Pa). Taking this into account, pressure values above the atmospheric pressure will take positive values, while those below the atmospheric pressure will be negative.

When the flow meets the underfloor surface, it undergoes a small increase in pressure due to the light stagnation that the air experiences when hitting the body.

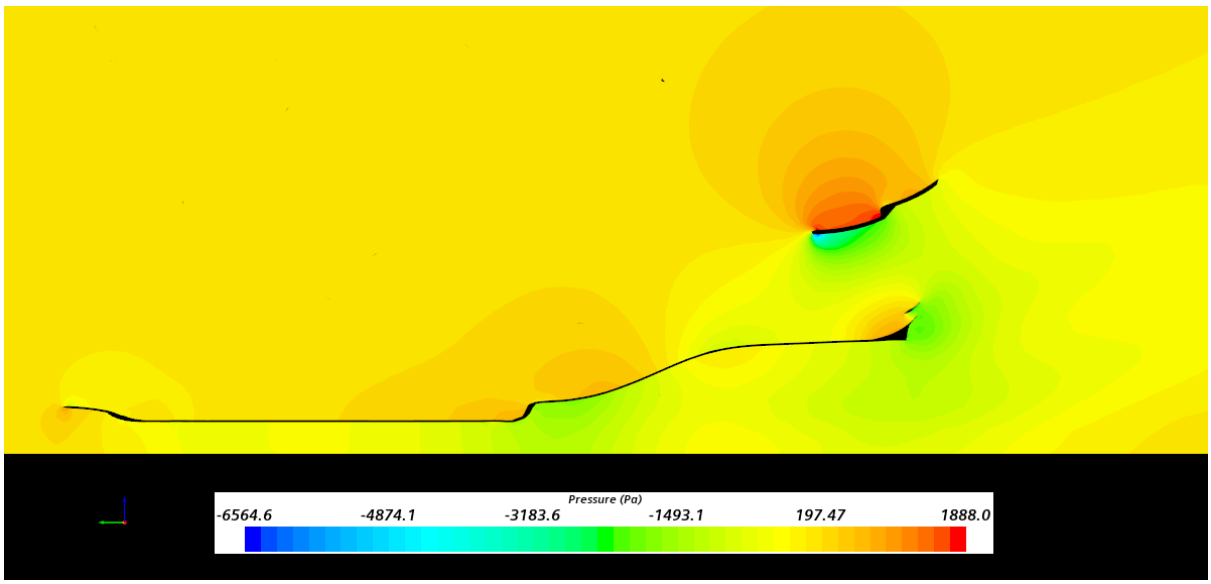

Figure 5.11: Pressure contours of the whole assembly (10 s).

Once it enters the volume between the underfloor and the track, pressure gradually decreases until the underfloor begins to expand to form the diffusers. As Figure 5.12 represents, a minimum relative pressure of around -2000 Pa is reached, originating a considerable suction region in the underfloor. From this point on, pressure increases again to recover its initial value. Then, it exits the diffusers and adopts the value of ambient pressure again.

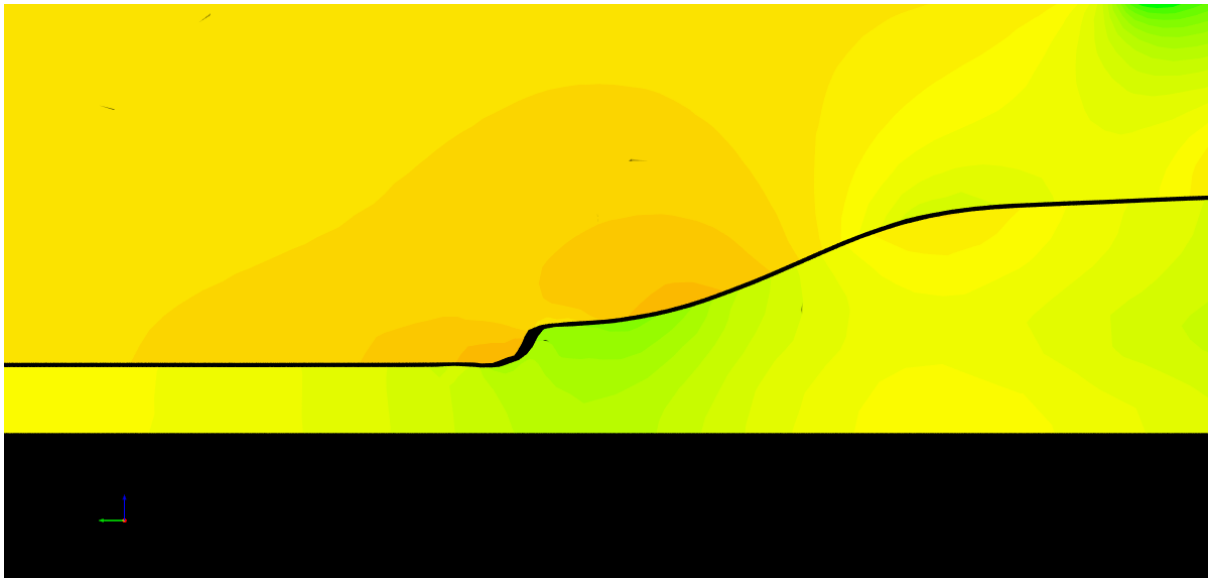

Figure 5.12: Low pressure region between the track and the underfloor of the car (10 s).

The flow passing through the rear wing experiences a strong pressure gradient, as shown in Figure 5.13. On the one hand, a huge pressure drop in the underside of the reverse airfoil

takes place, due to the velocity increase resulting from the flow expansion. On the other hand, pressure passing over this surface increases as a consequence of the flow being compressed. This pressure difference generates high downforce levels.

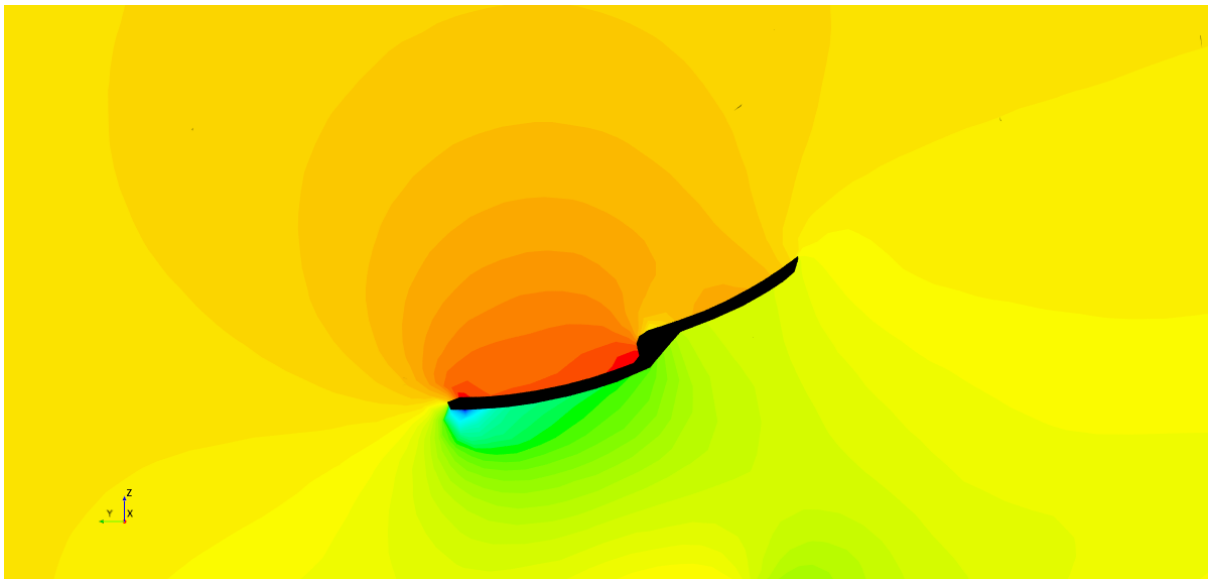

Figure 5.13: Pressure gradient originated in the rear wing (10 s).

5.3.3 Vorticity

Vorticity is a vector quantity that describes the amount of "circulation" or "rotation" (or more strictly, the local angular rate of rotation) of a fluid parcel. It is an important concept in order to quantify the rotational behavior of a fluid element. In the case of this project, it is useful for identifying those areas where the flow becomes more turbulent due to the influence of the aerodynamic elements that are being studied. In these areas, the flow loses its laminar nature and swirls originate.

Figure 5.14 shows four scenes of vorticity, each one considering a different range of vorticity magnitude, after 10 seconds of simulation. From these images, it can be concluded that the range between 150 /s and 200 /s is associated to the most severe vorticity, which is a consequence of the rear wing's shape, and extends a small distance downstream this device. After some meters, this vorticity weakens and its intensity drops down to values below 100 /s until it attenuates to almost 0 /s.

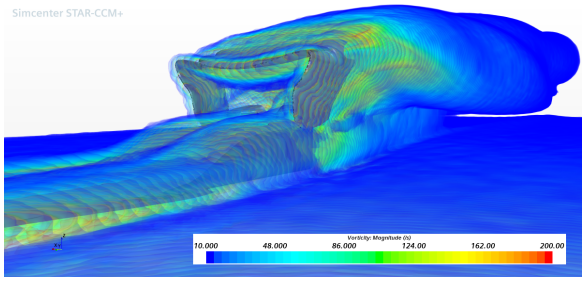

(a) 10 /s to 200 /s.

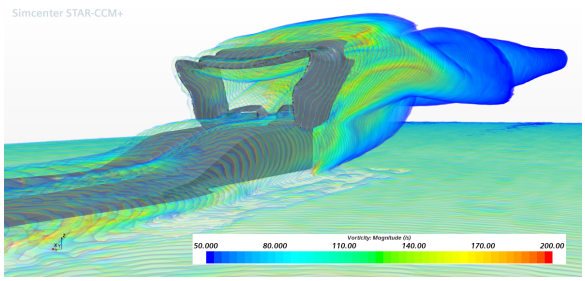

(b) 50 /s to 200 /s.

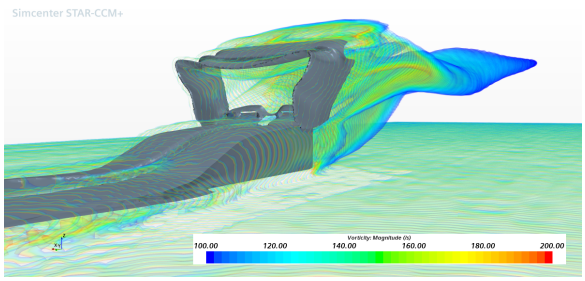

(c) 100 /s to 200 /s.

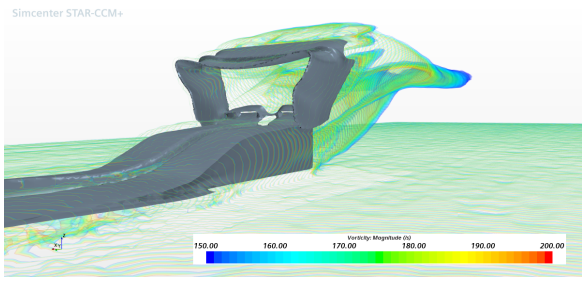

(d) 150 /s to 200 /s.

Figure 5.14: Vorticity scenes downstream the Formula 1 car (10 s).

5.3.4 Turbulent Viscosity Ratio

The Turbulent Viscosity Ratio (TVR) is defined as the ratio of turbulent viscosity to molecular viscosity. It allows to model turbulent flows by characterizing the behavior of turbulent eddies and their effect on the viscosity of the fluid. High TVR values suggest that turbulence dominates the flow behavior, whereas low TVR values indicate that the flow has a more laminar and less chaotic nature. Figure 5.15, Figure 5.16, Figure 5.17 and Figure 5.18 plot the TVR evolution downstream the car at several instants.

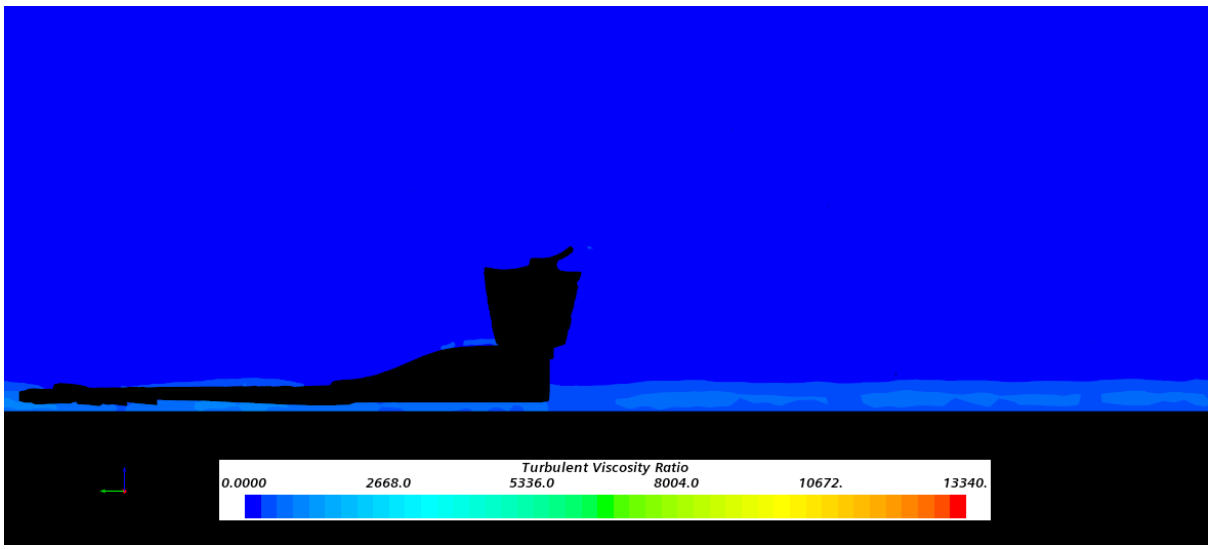

Figure 5.15: TVR contours downstream the vehicle (0.1 s).

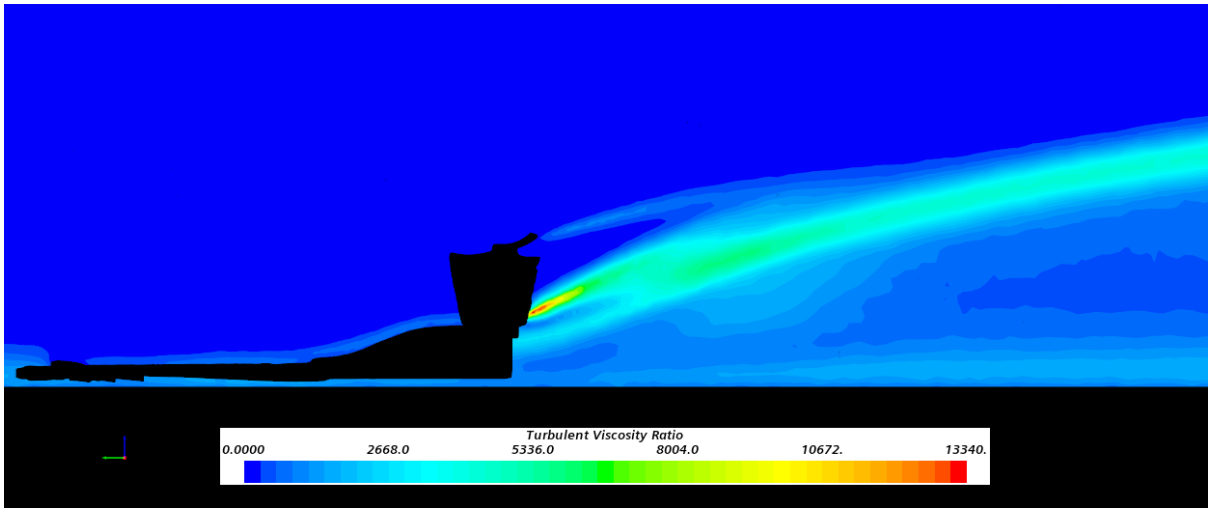

Figure 5.16: TVR contours downstream the vehicle (2.5 s).

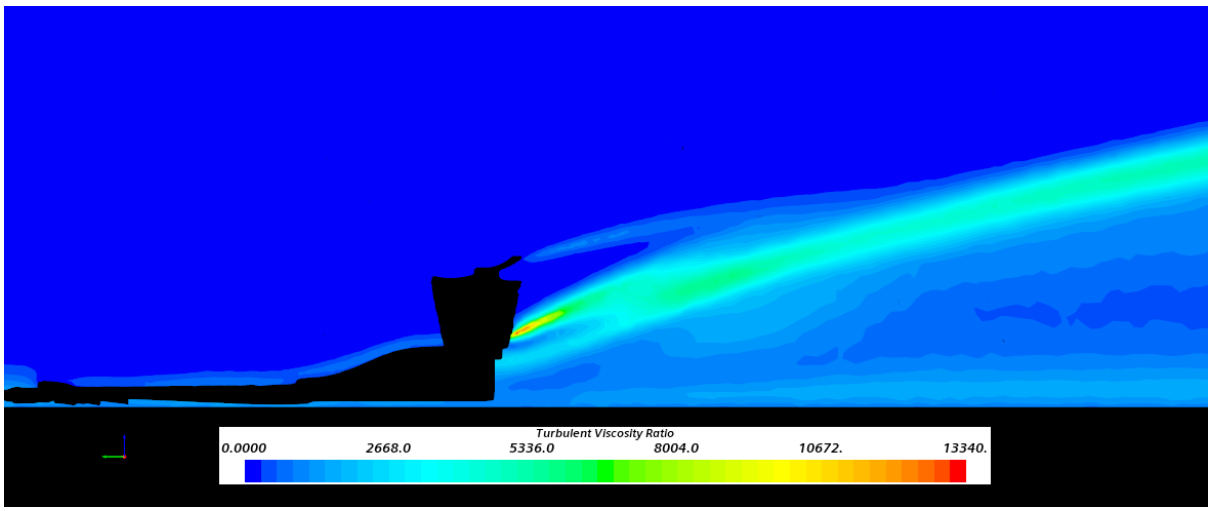

Figure 5.17: TVR contours downstream the vehicle (5 s).

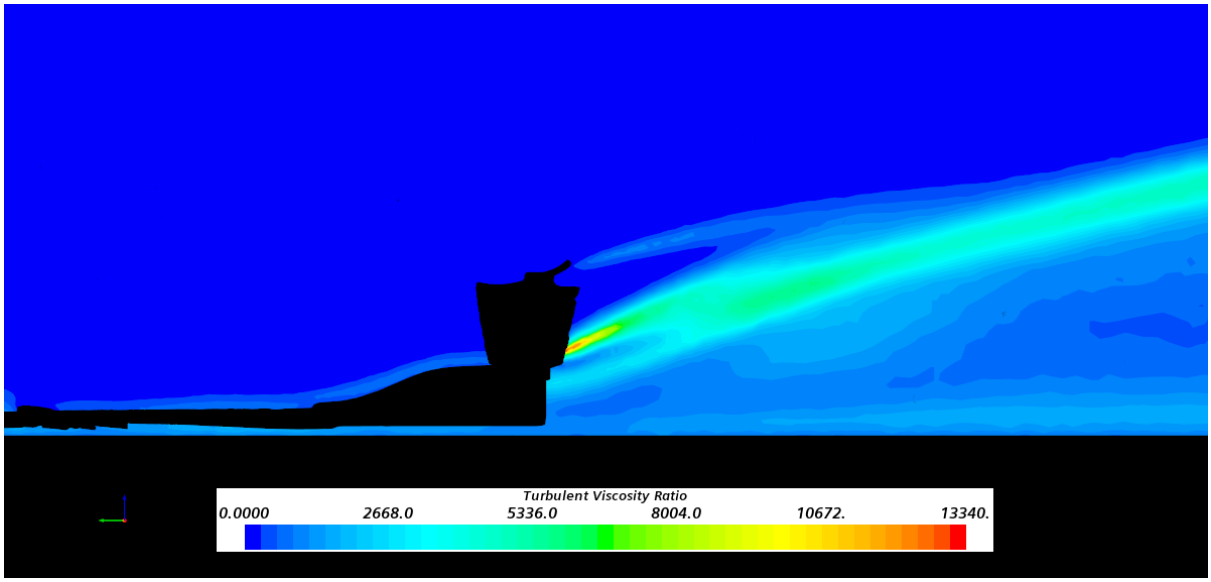

Figure 5.18: TVR contours downstream the vehicle (10 s).

5.3.5 Streamlines

Streamlines are a curves tangential to the flow velocity direction. They are the path of imaginary particles suspended in the fluid and carried along with it. Figure 5.19 and Figure 5.20 present the path followed by streamlines downstream the Formula 1 car, just after exiting the underfloor and joining the flow coming from the rear wing, after 10 seconds of simulation. It can be appreciated how the pressure difference between the underside and the top side of the rear wing leads to the formation of vortices when both airflows meet after leaving the rear wing.

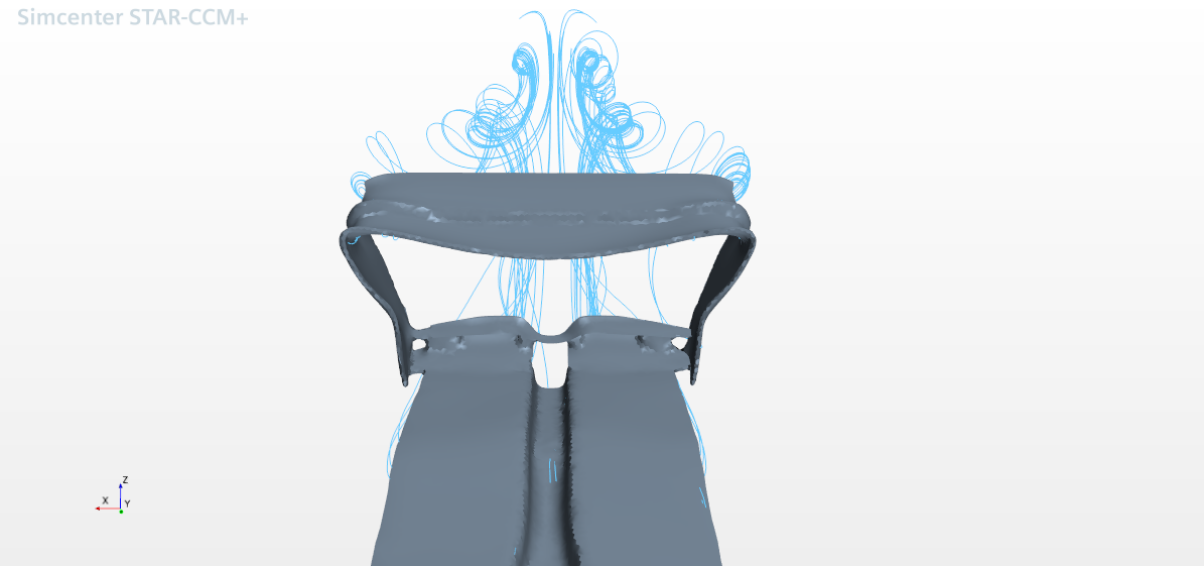

Figure 5.19: Vortices formed downstream the vehicle (10 s).

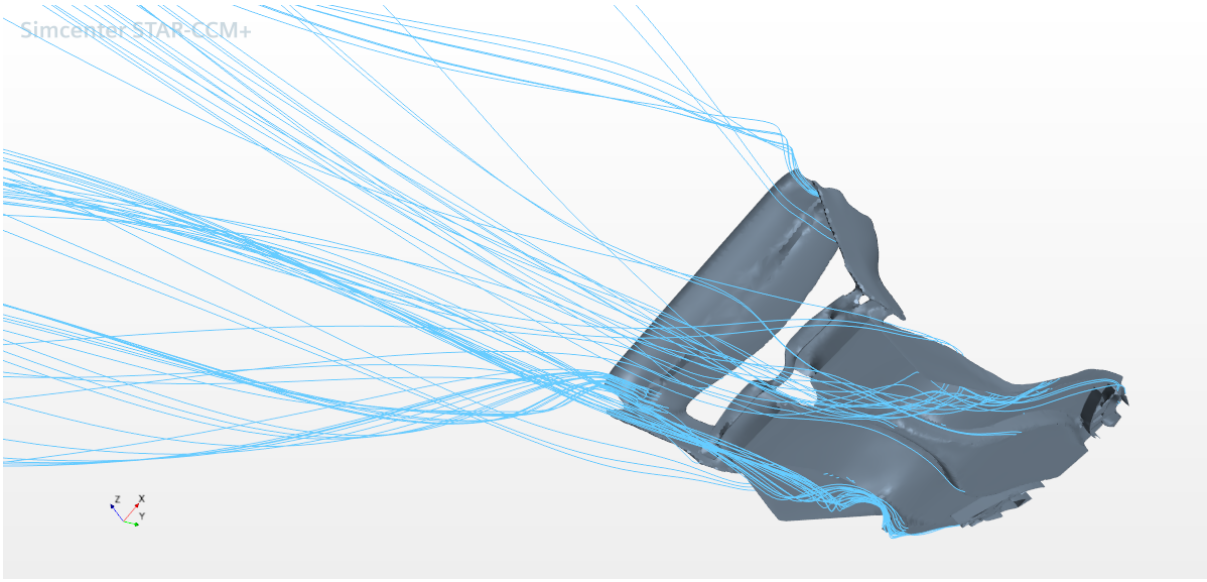

Figure 5.20: Streamlines leaving the underfloor and the rear wing of the vehicle (10 s).

5.4 Drag

The total drag force generated by the whole aerodynamic set, including the underfloor, beam wing and rear wing, is depicted in Figure 5.21.

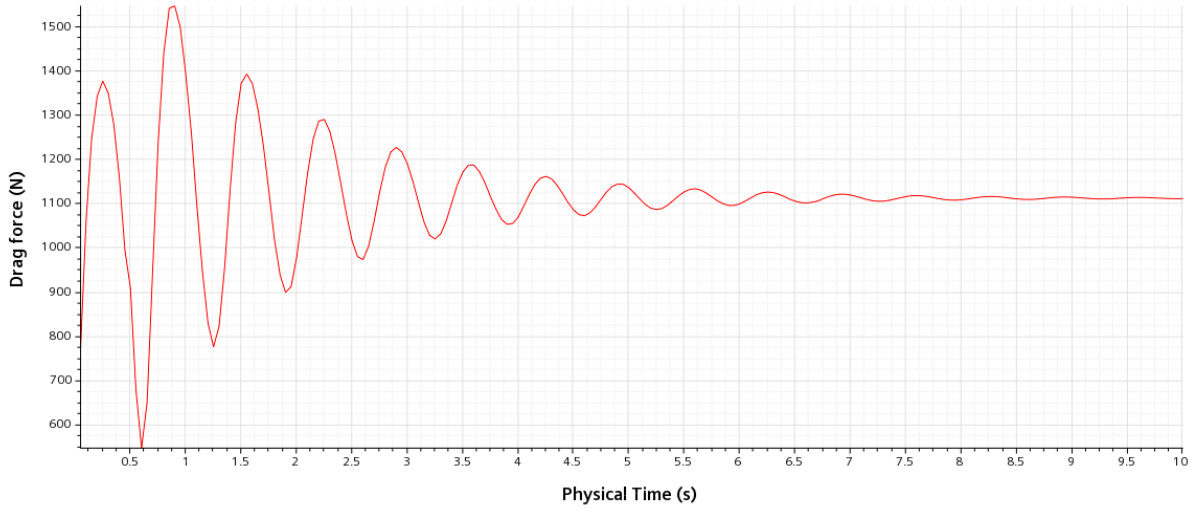

Figure 5.21: Evolution of the drag generated by the high-downforce configuration in 10 s.

It can be observed that the value of drag oscillates during the first seconds of the simulation, due to the unsteady nature of the studied situation, characterized by vortex shedding and instability of the flow properties. Then, the flow stabilizes and so does the produced drag, which takes a value around 1120 N.

More precisely, the drag report provided by *STAR-CCM+* after 10 seconds gives:

Drag= 1110.352 N

5.5 Downforce

The evolution of the total downforce generated by the aerodynamic elements is plotted in Figure 5.22.

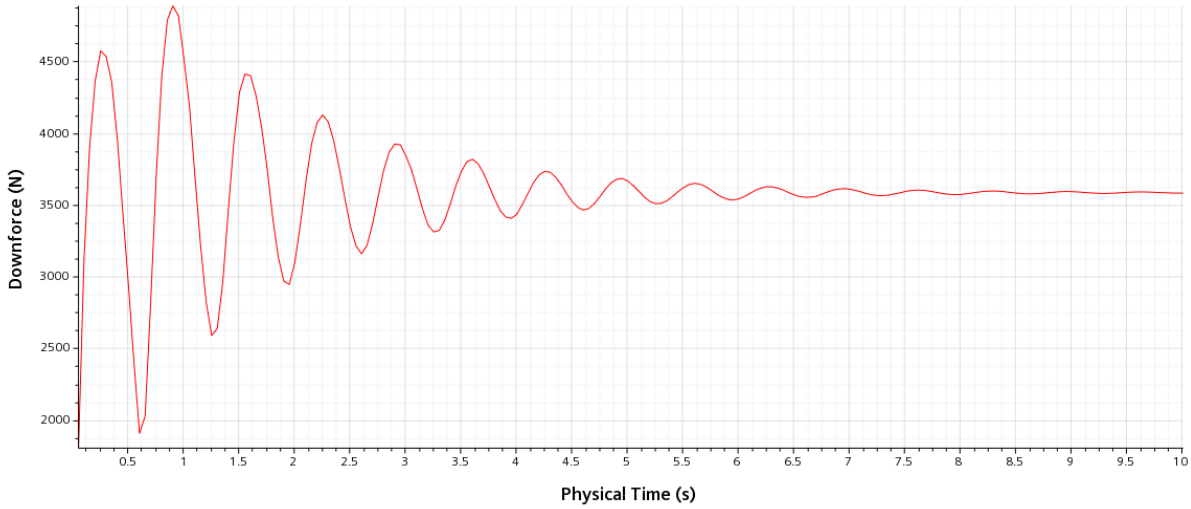

Figure 5.22: Evolution of the downforce generated by the high-downforce configuration in 10s.

Again, the value of downforce oscillates until stabilizing after some seconds. The final value at 10 seconds is:

Downforce = 3582.013 N

6 Low - drag case

6.1 Meshing

The meshing process followed for the low-drag case is essentially the same as the one followed for the high-downforce case, although with some variations.

6.1.1 Models

The meshing models chosen for this analysis are the following:

- Polyhedral mesher.
- Surface remesher.
- Surface wrapper.

6.1.2 Reference values

The main parameters defining the mesh are:

- Base Size: 0.05 m
- Surface Growth Rate: 1.3
- Relative Minimum Size: 30
- Relative Target Size: 100

6.1.3 Diagnostics

- Cells: 6576062
- Faces: 47647407
- Verts: 41393174

An image of the resulting mesh is depicted in Figure 6.1

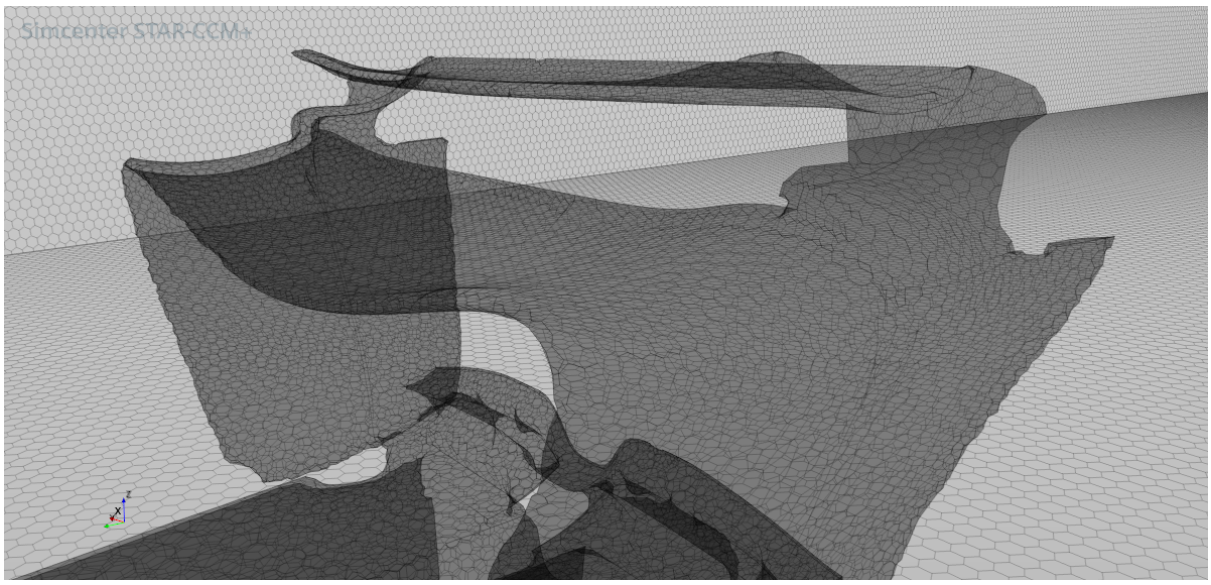

Figure 6.1: Mesh detail of the low-drag case geometry.

6.2 Analysis of residuals

The evolution of residuals is presented in Figure 6.2. As commented in subsection 5.2, the residuals plot acquires a periodic and fluctuating behaviour, proper to unsteady flow simulations.

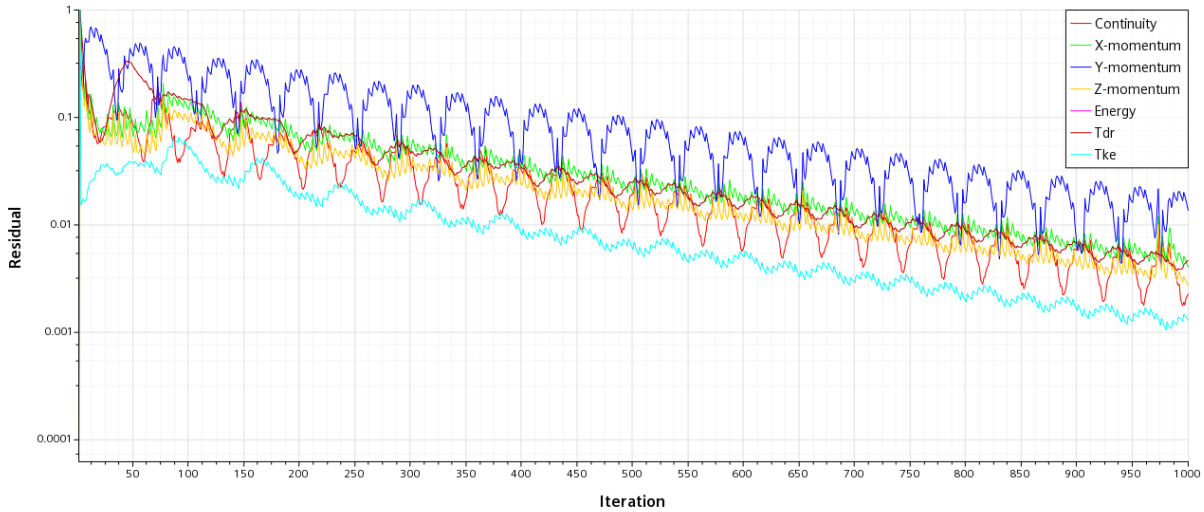

Figure 6.2: Residuals plot for the low-drag case.

After carrying out 1000 iterations, the residuals of continuity, x-momentum, z-momentum,

tdr and tke are of the order of 10^{-3}. Those of y-momentum are of the order of 10^{-2}, and those of energy are null due to the isothermal condition. These are relatively acceptable values for assuming a stabilized flow after 10 seconds of simulation.

6.3 Results

6.3.1 Velocity

Figure 6.3, Figure 6.4 and Figure 6.5 show the velocity contours at 0.1 s, 2.5 s and 5 s, respectively.

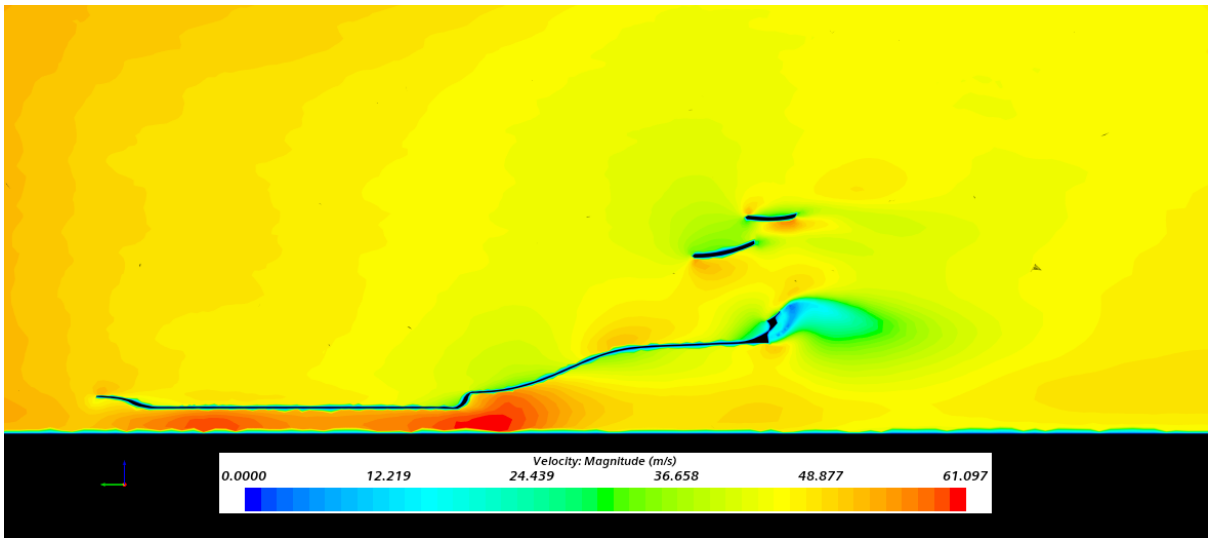

Figure 6.3: Velocity magnitude contours of the whole assembly (0.1 s).

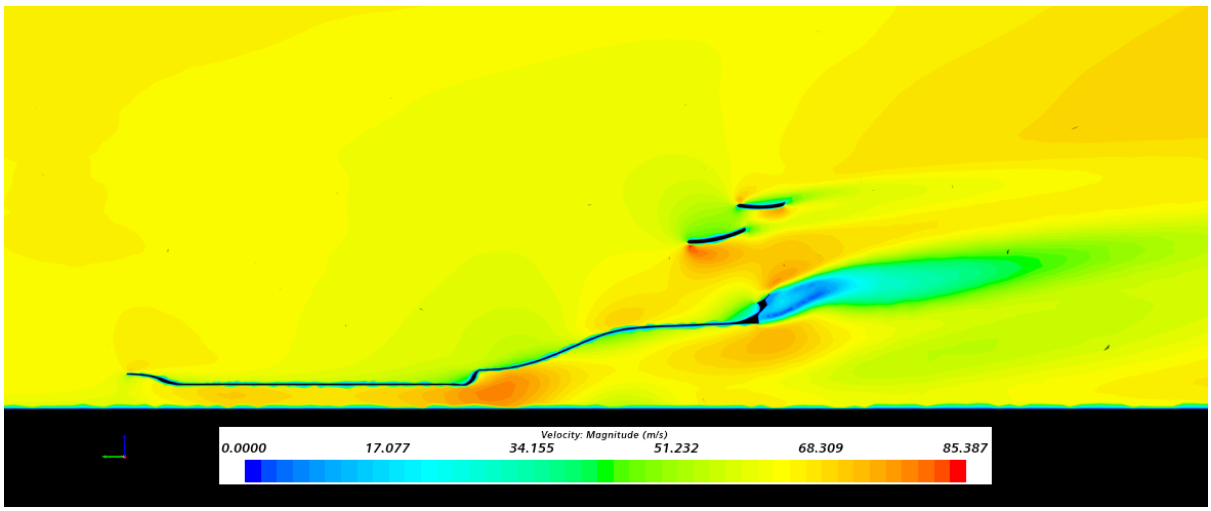

Figure 6.4: Velocity magnitude contours of the whole assembly (2.5 s).

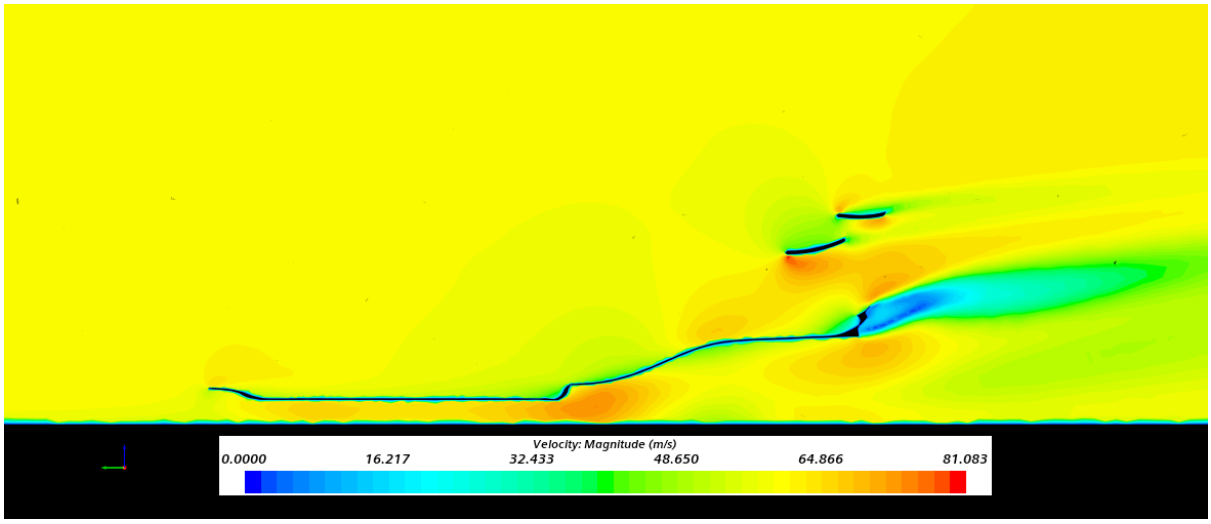

Figure 6.5: Velocity magnitude contours of the whole assembly (5 s).

As it can be observed, the velocity field is yet not completely stabilised at these time instants. In particular, when just 0.1 seconds have passed, the flow has not already reached 60 m/s.

At 10 seconds, the flow approaches the front of the underfloor at 60 m/s, established as the inlet velocity. The airflow between the underfloor and the ground behaves fundamentally the same as in the high-downforce situation, as represented in Figure 6.6.

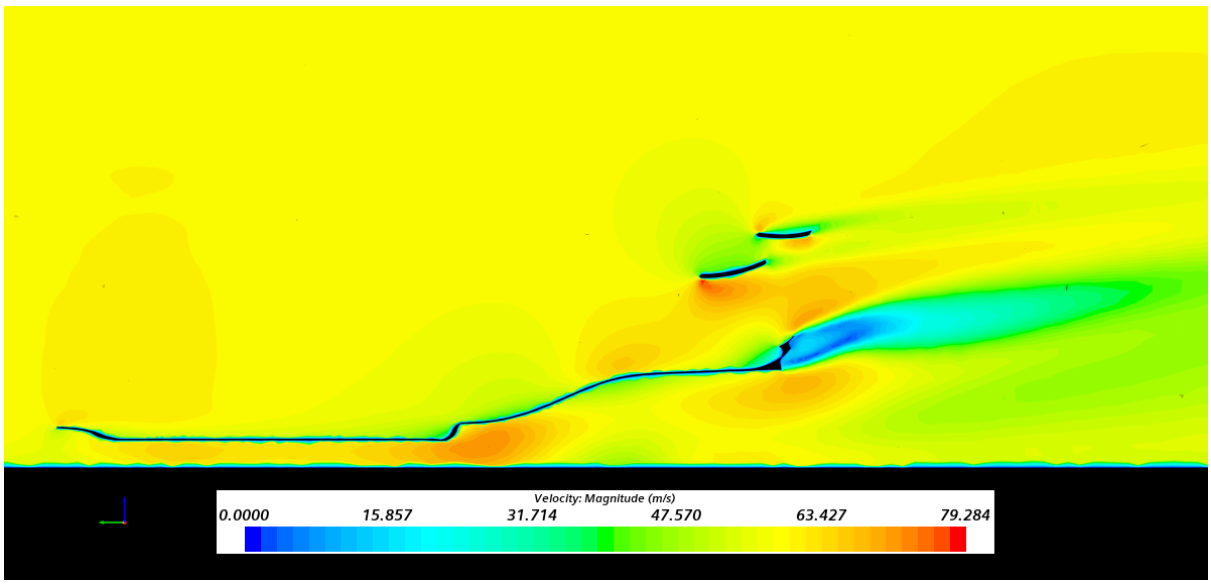

Figure 6.6: Velocity magnitude contours of the whole assembly (10 s).

From the beginning of the underfloor till the beginning of the diffuser, the flow is accelerated along the Venturi channels, up to values close to 80 m/s, as shown in Figure 6.7. Then, the flow gradually loses velocity as it passes through the diffusers and exits the car.

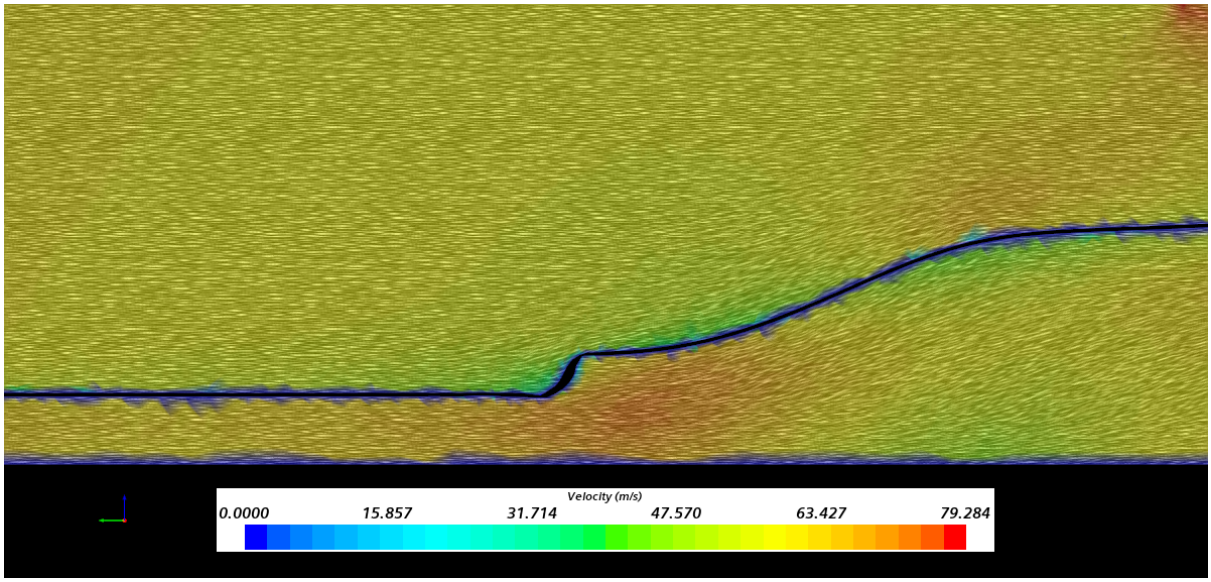

Figure 6.7: Detail of the velocity magnitude and direction between the car's underfloor and the track (10 s).

In this case, the decrease in the frontal surface encountered by the air when reaching the rear wing (due to the activation of the DRS) leads to a smaller velocity decrease downstream the vehicle, as Figure 6.8 shows.

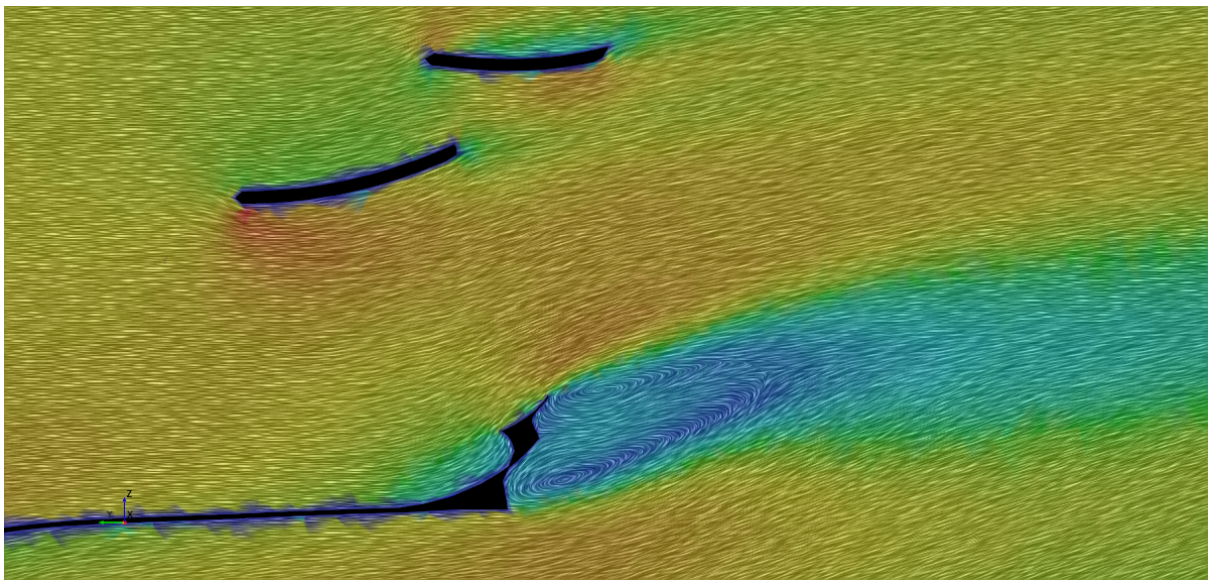

Figure 6.8: Detail of the velocity magnitude and direction in the car's rear wing and beam wing (10s).

6.3.2 Pressure

The pressure distribution of the configuration is depicted in Figure 6.9, Figure 6.10 and Figure 6.11 for several time instants.

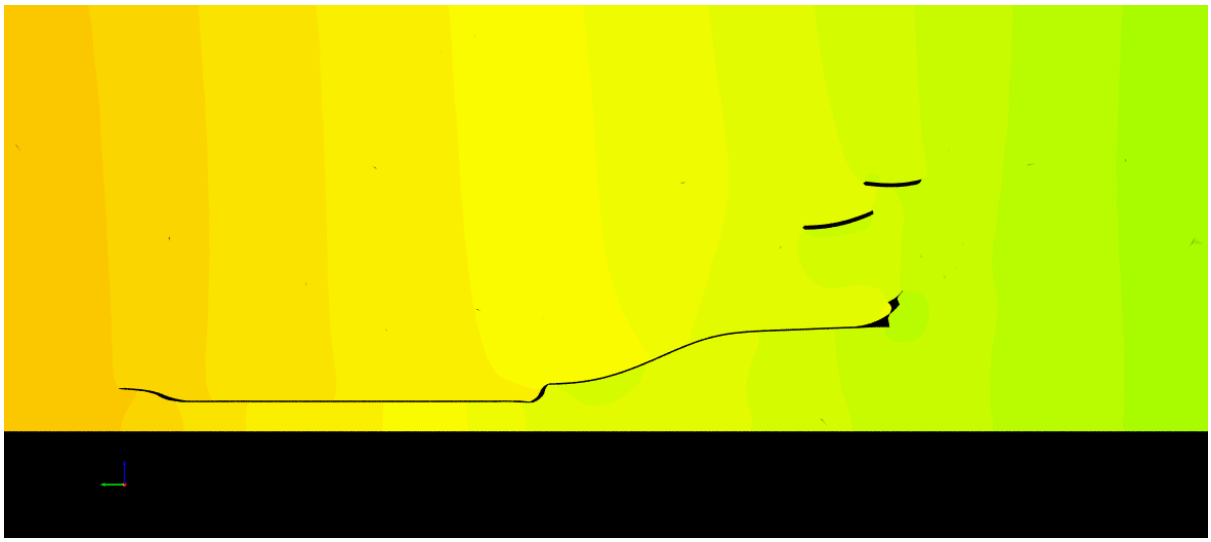

Figure 6.9: Pressure contours of the whole assembly (0.1 s).

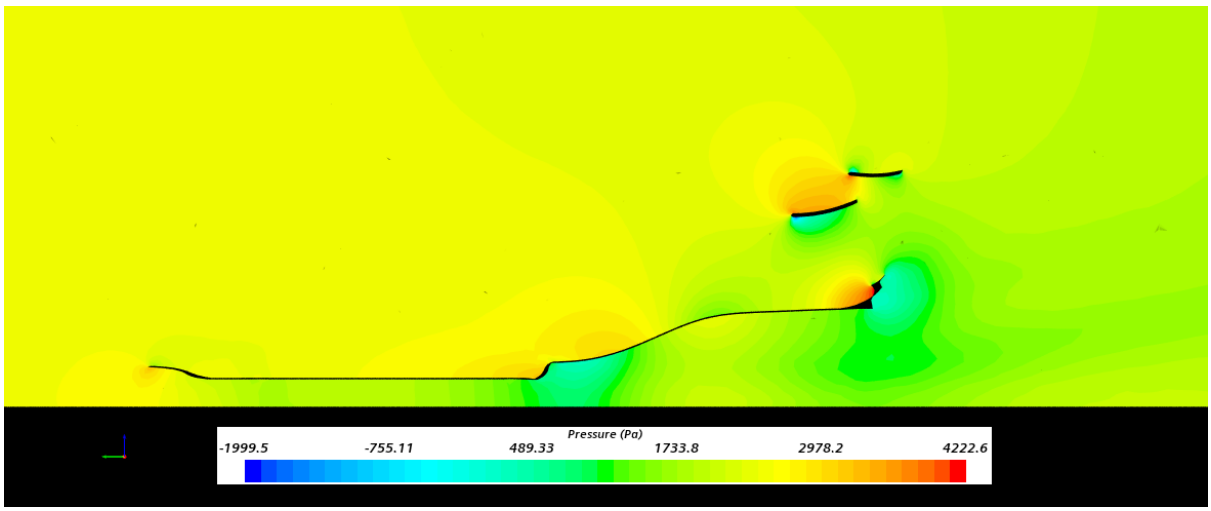

Figure 6.10: Pressure contours of the whole assembly (2.5 s).

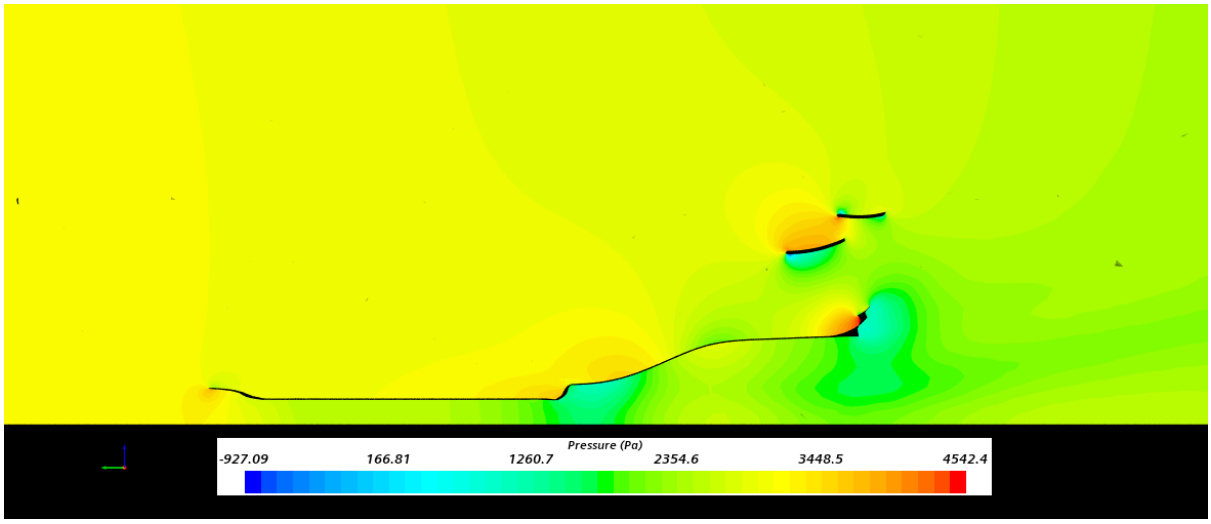

Figure 6.11: Pressure contours of the whole assembly (5 s).

Figure 6.12 depicts the pressure contours of the airflow when it encounters the F1 car after 10 seconds have passed, where it is essentially stable.

As in the high-downforce case, the pressure of the flow slightly increases when reaching the underfloor surface, due to the stagnation that the it suffers when hitting the body.

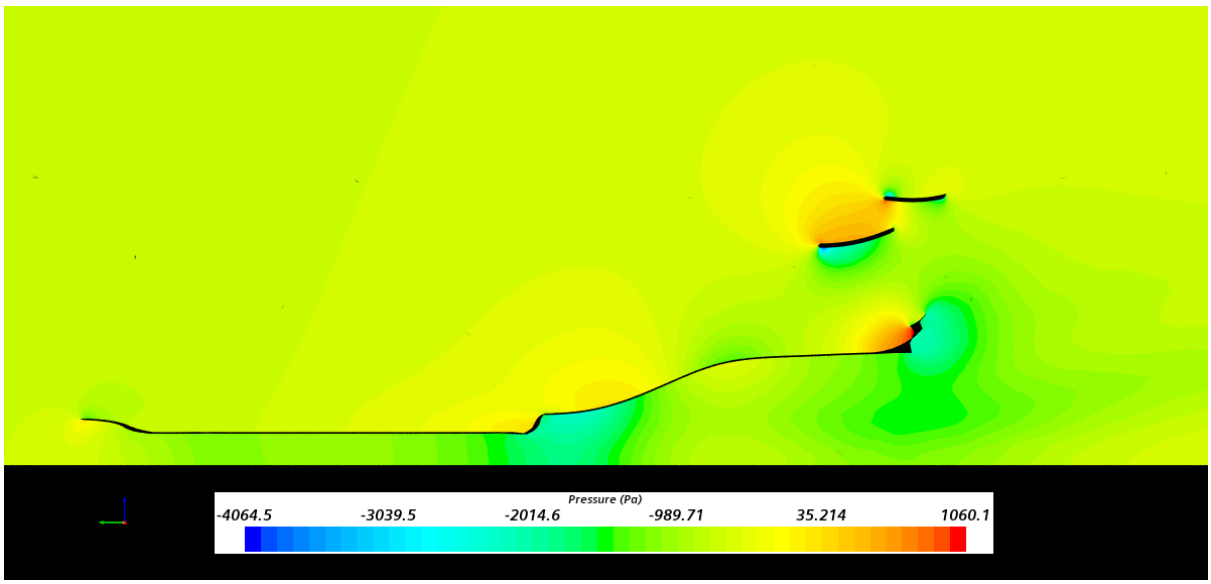

Figure 6.12: Pressure contours of the whole assembly (10 s).

Once the airflow enters the volume between the underfloor and the track, pressure gradually decreases until the underfloor begins to expand. Figure 6.13 depicts the minimum pressure region, where values of relative pressure around -2000 Pa are reached. Then it starts to grow, until it exits the diffusers and acquires the value of ambient pressure again.

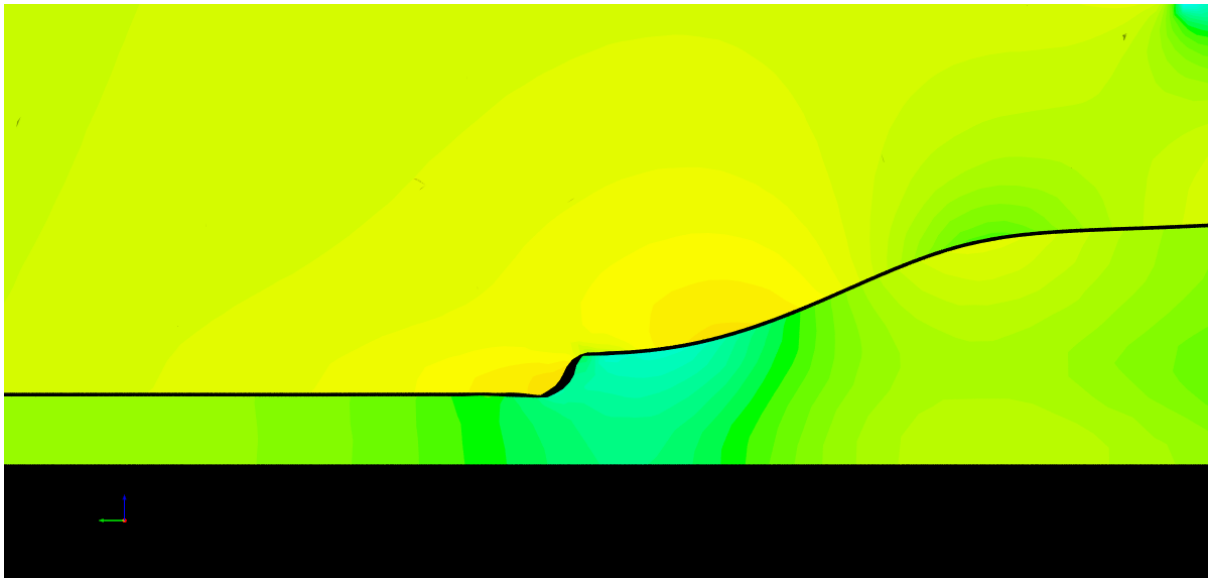

Figure 6.13: Low pressure region between the track and the underfloor of the car (10 s).

The most noticeable difference with the high-downforce case takes place im the rear wing. In this case, the DRS system is active, meaning that the adjustable flap of the rear wing is in horizontal position. As Figure 6.14 presents, in this situation the rear wing produces down-

force only by means of its fix surface, which remains always curved with the same angle, due to the pressure gradient that it generates. Nevertheless, the flap in horizontal position does not contribute to downforce generation, given that pressure in its upper side and in its lower side is essentially the same.

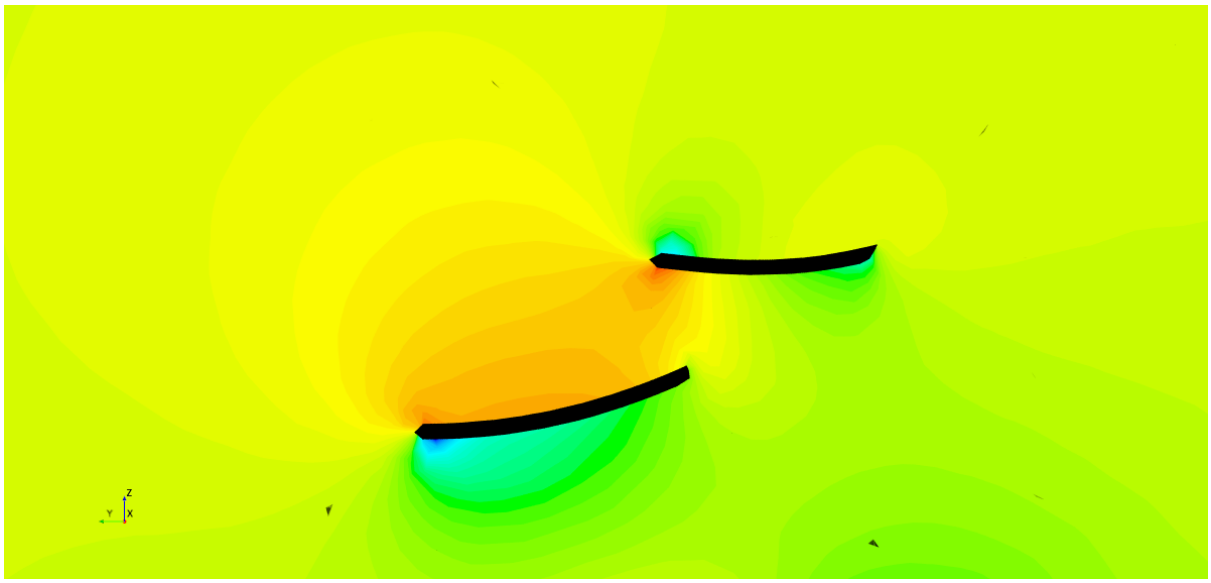

Figure 6.14: Pressure gradient originated in the rear wing and DRS flap (10 s).

6.3.3 Vorticity

Figure 6.15 shows four scenes of vorticity, each one considering a different range of vorticity magnitude. As in the high-downforce case, it can be appreciated that the range between 150 /s and 200 /s is related to the most intense vorticity, which originates because of the rear wing's shape, and extends a small distance downstream the car. Then it loses its strength and drops down to values below 100 /s until it attenuates.

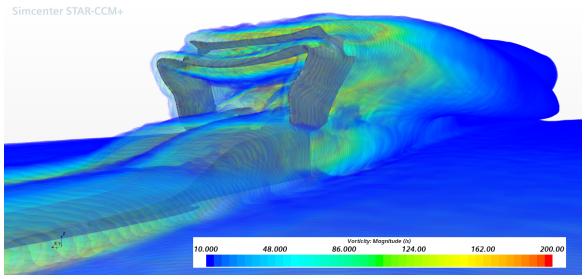

(a) 0 /s to 200 /s.

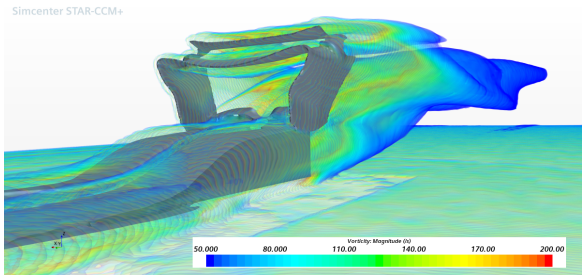

(b) 50 /s to 200 /s.

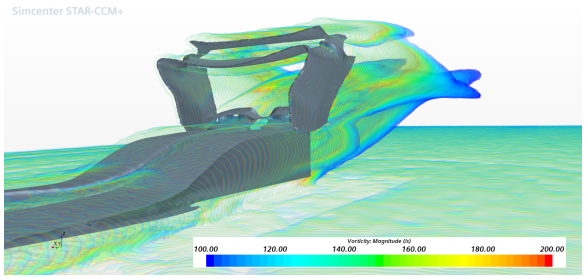

(c) 100 /s to 200 /s.

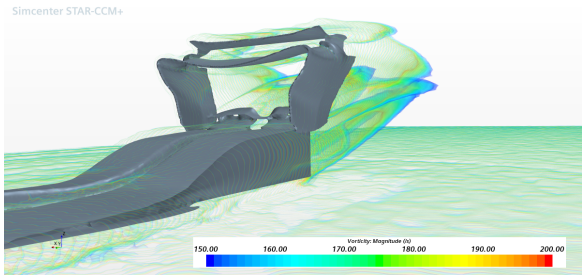

(d) 150 /s to 200 /s.

Figure 6.15: Vorticity scenes downstream the Formula 1 car (10 s).

6.3.4 Turbulent Viscosity Rate

TVR follows a similar behaviour as in the high-downforce situation. The beam wing is the main element provoking turbulence, leaving a wake of non-laminar flow that extends several meters away from the car. Yet, in this case, the reduction of drag as a consequence of DRS activation avoids the formation of the secondary wake that formed in the high-downforce case downstream the rear wing, which eventually joined the bigger wake generated by the beam wing. Figure 6.16, Figure 6.17, Figure 6.18 and Figure 6.19 plot this scenario at different moments.

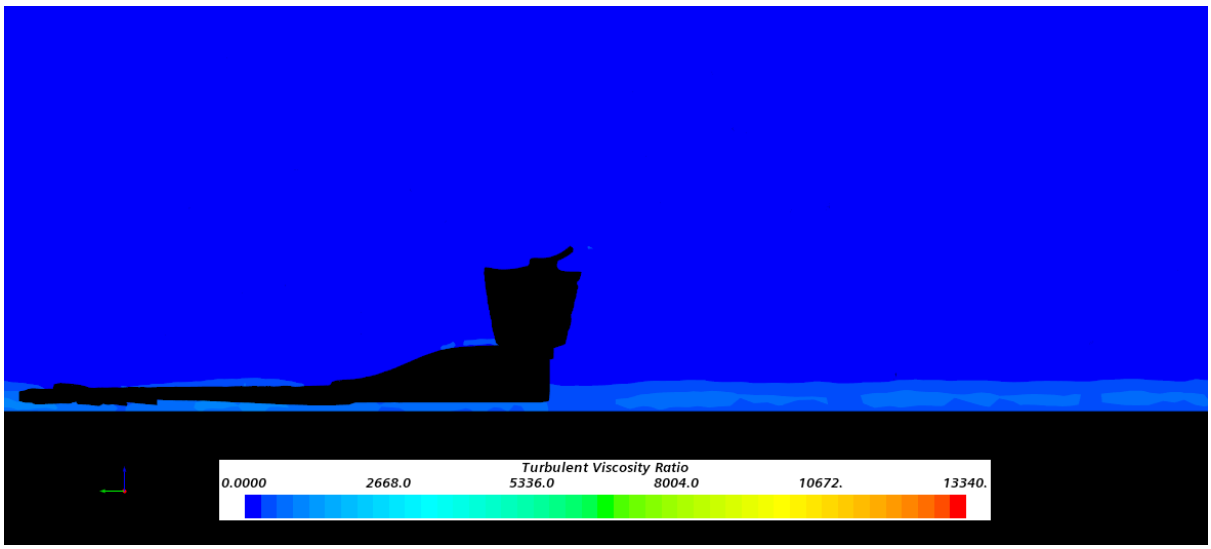

Figure 6.16: TVR contours downstream the vehicle (0.1 s).

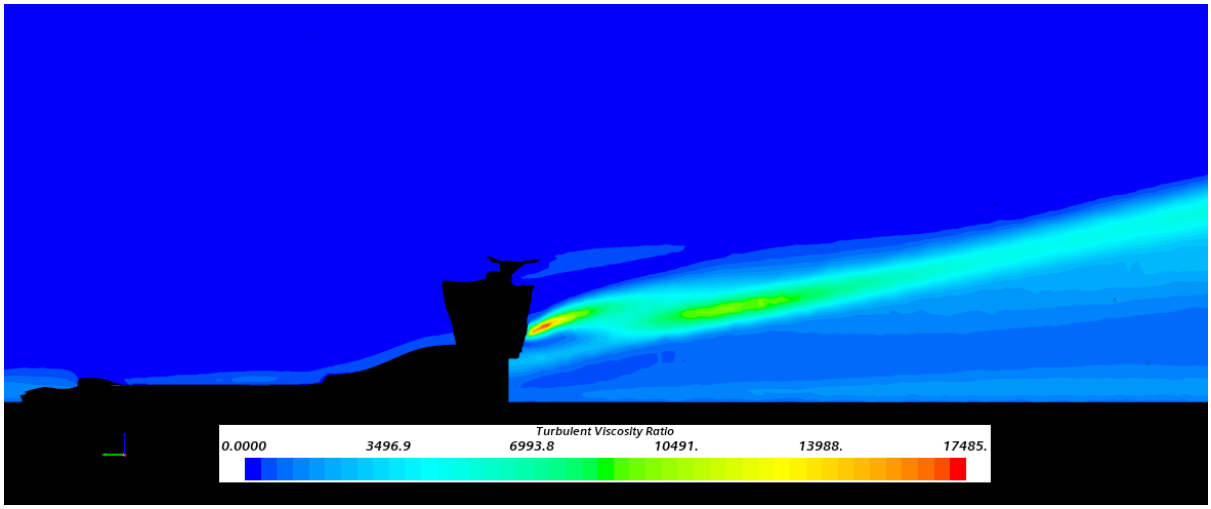

Figure 6.17: TVR contours downstream the vehicle (2.5 s).

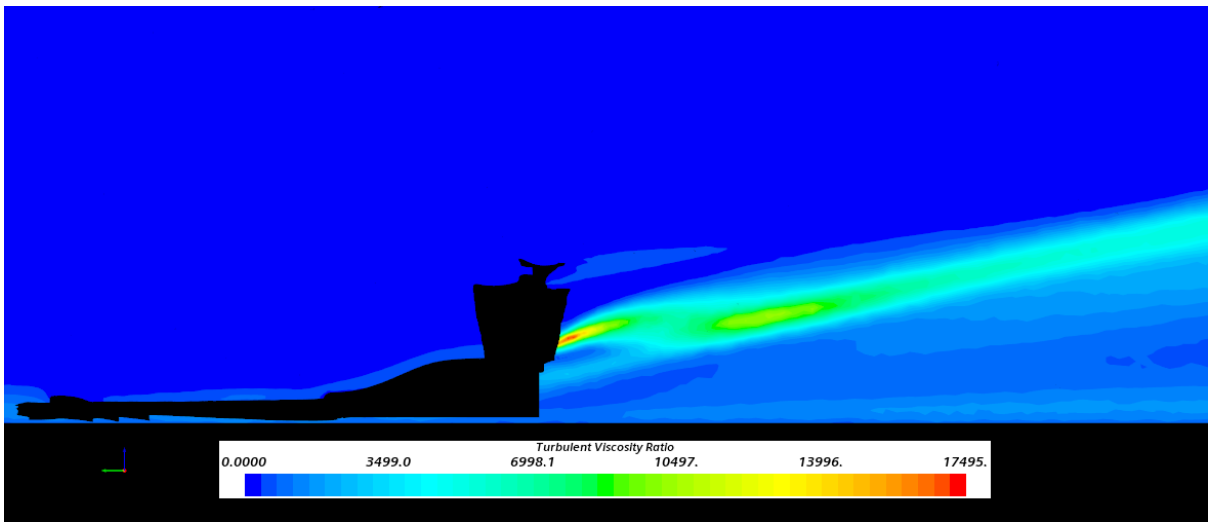

Figure 6.18: TVR contours downstream the vehicle (5 s).

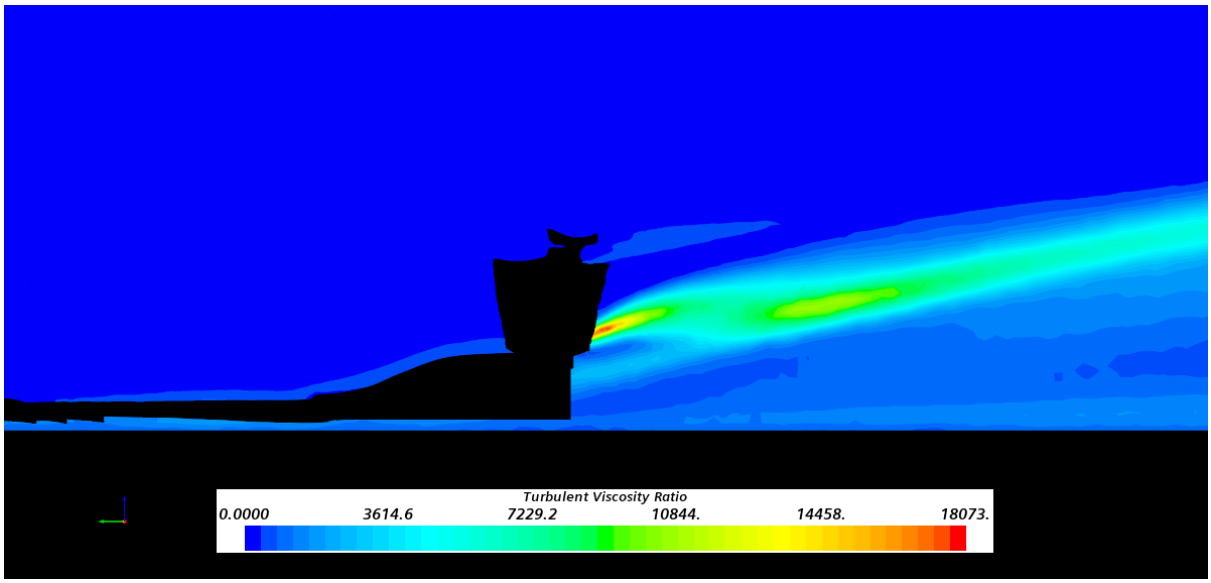

Figure 6.19: TVR contours downstream the vehicle (10 s).

6.3.5 Streamlines

The path of the airflow is represented by the streamlines depicted in Figure 6.20 and Figure 6.21, as well as the vortices that originate downstream the vehicle.

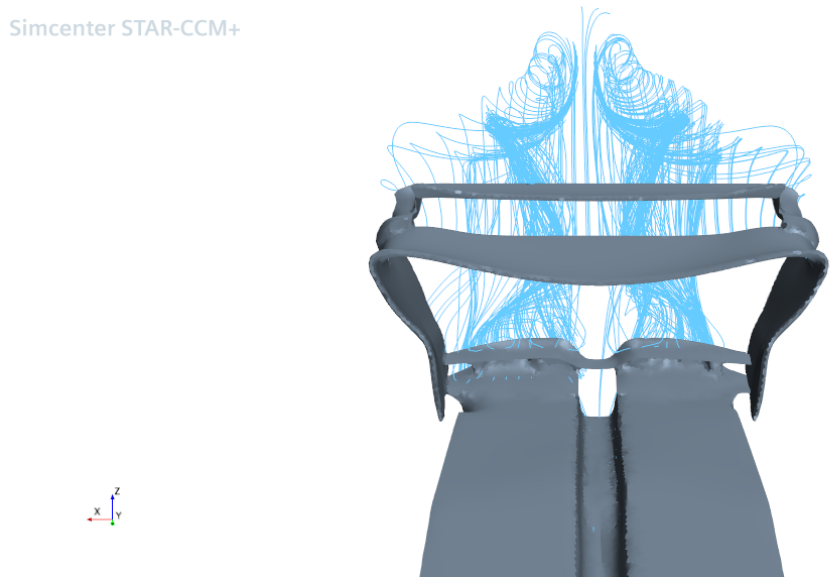

Figure 6.20: Vortices formed downstream the vehicle.

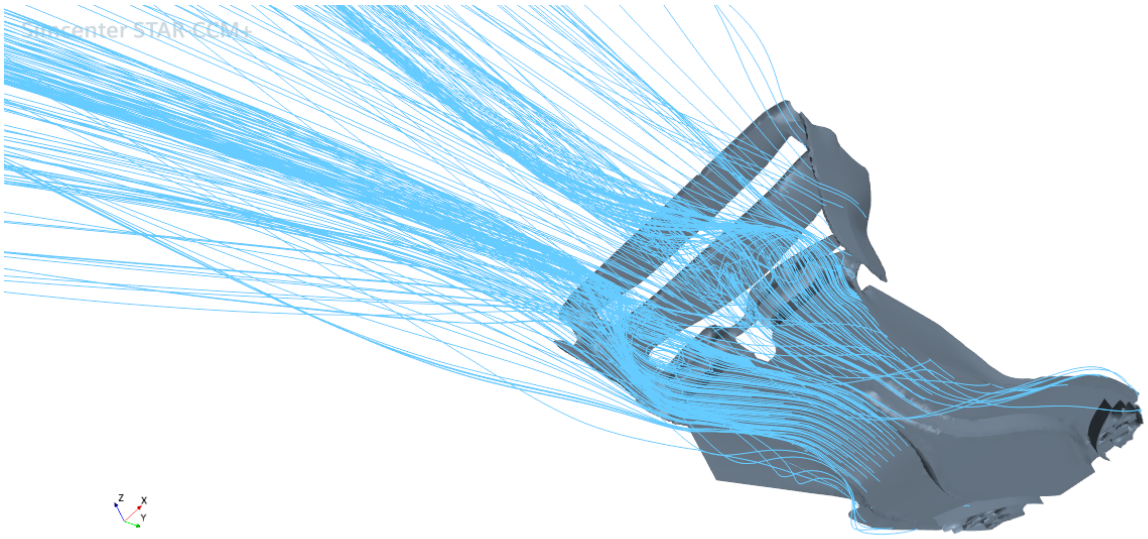

Figure 6.21: Streamlines leaving the underfloor and the rear wing of the vehicle.

6.4 Drag

The evolution of the generated drag over time is depicted in Figure 6.22.

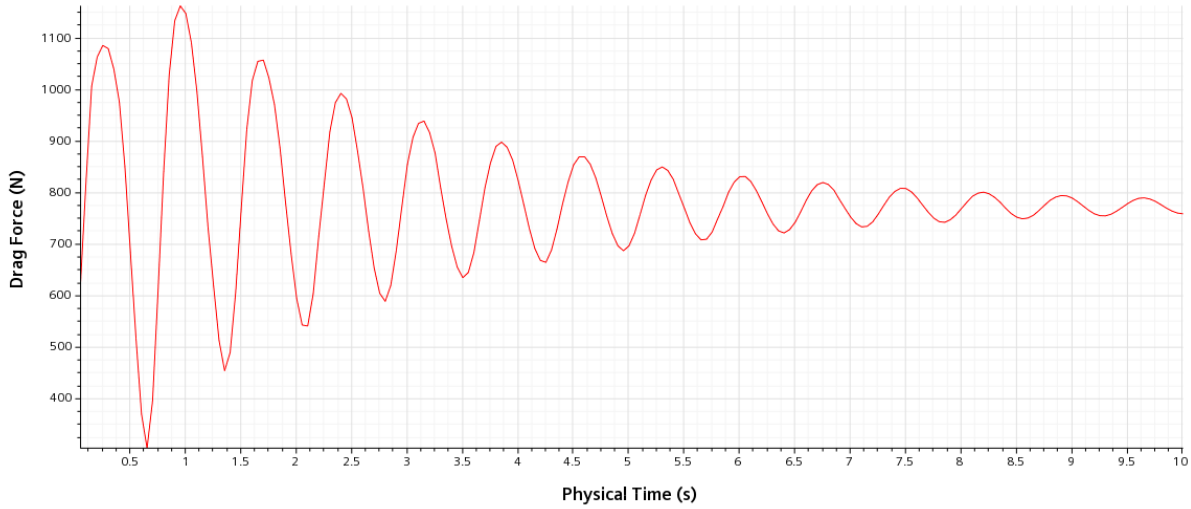

Figure 6.22: Evolution of the drag generated by the low-drag configuration in 10 s.

In contrast to the drag plot of the high-downforce case (presented in subsection 5.4), the flow takes more time to reach a stable behaviour. Hence, the drag force remains oscillating for a longer time, until it starts to stabilize around 750 N. The exact value after 10 seconds of simulation is:

Drag= 754.756 N

6.5 Downforce

Figure 6.23 plots the evolution of the drag generated by the aerodynamic assembly.

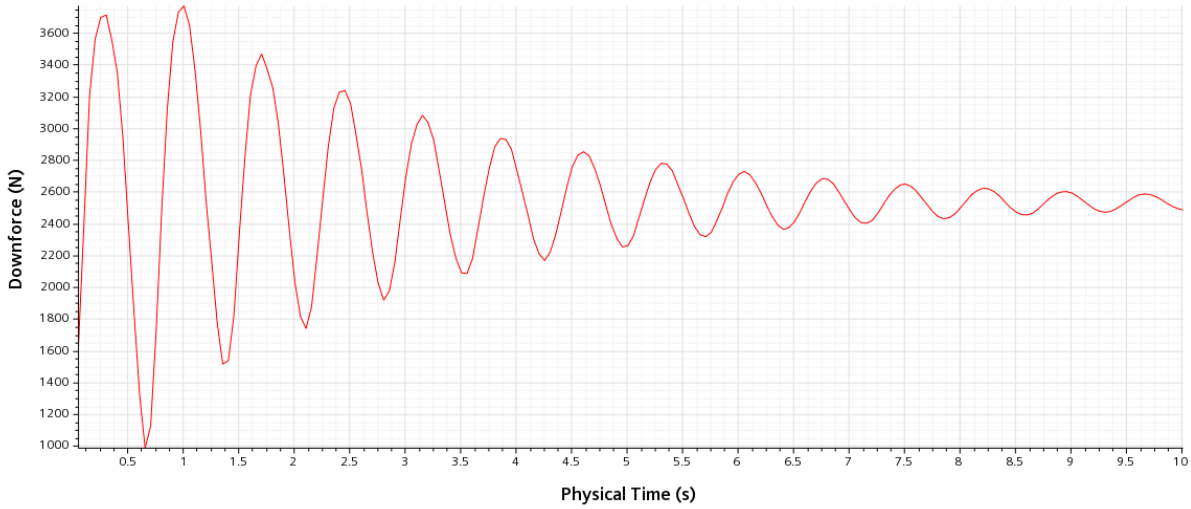

Figure 6.23: Evolution of the drag generated by the low-drag configuration in 10 s.

The downforce plot also exhibits a more instable behaviour than the downforce plot of the high-downforce case (presented in subsection 5.5). After some seconds fluctuating, the value of this force stabilizes around 2500 N. After 10 seconds have passed, the value of downforce is:

Downforce = 2478.192 N

7 Concluding remarks

The development of this project leads to a series of observations and comments.

First of all, the understanding of the importance that the surfaces and components of a Formula 1 car have on the vehicle's aerodynamic behaviour. In particular, the devices that have been studied in detail in this project correspond to the rear section of the car. These have been found to be crucial in the management of downforce and drag in the racing context. On the one hand, the vehicle's underfloor geometry (which incorporates two Venturi channels) allows to generate suction between the car and the track, leading to a pressure gradient that provides a perpetual downforce generation at high racing speeds. Thanks to the beam wing located just above the underfloor diffusers' exit, the airflow expands and recovers its initial pressure more smoothly when it leaves the car. On the other hand, the rear wing proves its capacity of generating more or less downforce depending on the pilot's needs, by means of the DRS system that it incorporates. In other words, it can make the car be more attached to the ground in detriment of an increased drag (thus making it slower), or sacrifice this grip to produce less drag (making the car faster).

Another relevant point to highlight is the sequence followed to undergo the whole analysis. As the starting point, a CAD model representing the actual components of the car with accurate dimensions is required to get correct results close to reality. Then, a sufficiently large geometrical domain is established in STAR-CCM+, including the imported CAD in its interior. This domain is defined by its boundaries, which have to be chosen appropriately to recreate the racing environment. Next, the physical models are chosen to characterise the flow and the turbulence, as well as the initial conditions.

As for the nature of the project, it is clearly unsteady in both of the studied cases. The phenomena that arise in the vicinity of the car evolve over time until the flow stabilizes. This process takes longer for the low-drag case, when the DRS system is activated. This can be observed in the drag and downforce plots, which stabilize around a final value later than the drag and downforce curves of the high-downforce case. As well, in the residuals plot, where residuals are closer to zero in the high-downforce case than in the low-drag case after 10 seconds of simulation.

In terms if results, several magnitudes are analysed in the project. These remain essentially the same in both cases until reaching the rear wing. Here, the position of the DRS determines what happens downstream the car. On the one hand, when it is not active (high-downforce

case), the rear wing acts as a reversed airfoil, generating a high pressure gradient that translates into downforce. However, this configuration also leads to reversed flow and velocity loss just after the rear wing. On the other hand, when the DRS is active, a much lower pressure gradient is generated in the rear wing, so velocity losses downstream the car are reduced and drag is minimized. Vorticity is thus less intense than in the high-downforce case. As for turbulent viscosity rate (TVR), it is stronger in the region just after the beam wing, with a weaker secondary channel just after the beam wing. This secondary wake is more intense when the DRS is not active, even joining the main wake generated by the beam wing.

The fulfillment of Bernoulli's principle is also a remarkable point of the project. The inverse relation between velocity and pressure can be verified in the obtained scenes. Regions where the flow accelerates become low-pressure zones, whereas those where the flow loses velocity are characterised by higher pressure values.

Another relevant conclusion are the drag and downforce results obtained in each case. As for drag, the stabilised value after 10 seconds of simulation is 1100 N when the DRS is inactive, and 755 N when it is active. As for downforce, the obtained values after 10 seconds are 3582 N for the inactive DRS case and 2478 N for the active DRS case. This means that a 47.11 % more drag and a 44.54 % more downforce are generated by the inactive DRS configuration with respect to the active DRS case. These results are the expected ones, taking into account the difference in shape that the DRS position provokes in the rear wing of the F1 car, which also leads to differences in its aerodynamic behaviour.

All in all, this project results from the combination of both theoretical and practical fluid mechanics concepts, applied to the subsonic aerodynamics field. Its development has helped the author to acquire further knowledge both in the CAD and CFD environments, and to learn about the aerodynamics of F1 vehicles. Future research directions could involve a complete study of the car, including not only its rear aerodynamic surfaces but also the front ones. As well, making use of more powerful computational tools could lead to a significant reduction in simulation time, and consequently, to the possibility of getting quicker and more complete results.

References

[1] FIA. 2021 F1 rules status update [online]. URL: https://www.fia.com/news/f1-shape-things-come-2021-rules-status-update.

[2] Gary Anderson, Rosario Giuliana. What 2022-style F1 ground effect looks like [online]. URL: https://the-race.com/formula-1/gary-anderson-what-2022-style-f1-ground-effect-looks-like/.

[3] Matt Somerfield, Giorgio Piola. Why floor designs have become a key F1 battleground [online]. URL: https://www.autosport.com/f1/news/why-floor-designs-have-become-a-key-f1-battleground/10425142/.

[4] Mario Fernández Osma. The beam wing in Formula 1 [online]. URL: https://www.aerodinamicaf1.com/2022/03/el-beam-wing-en-la-f1/.

[5] Matt Somerfield, Giorgio Piola. Why new rear wing hints at change of F1 approach for Mercedes [online]. URL: https://www.motorsport.com/f1/news/why-new-rear-wing-hints-at-change-of-f1-approach-for-mercedes-/10438499/.

[6] Planet F1. What is F1's 'DRS' and how does it work? [online]. URL: https://www.planetf1.com/features/what-is-f1s-drs-and-how-does-it-work/.

[7] Sergio Ríos. Ferrari SF-23 [online]. URL: https://www.topgear.es/noticias/motorsport/ferrari-sf-23-coche-sainz-leclerc-iran-campeonato-1200926.

[8] Rich Opong, Luke Murphy. Why did F1 ban ground effect? [online]. URL: https://flowracers.com/blog/why-did-f1-ban-ground-effects/.

[9] Wikipedia. Lotus 78 [online]. URL: https://en.wikipedia.org/wiki/Lotus_78.

[10] Rich Opong. Dangers of the ground effect era [online]. URL: https://racingnews365.com/exclusive-marc-surer-relives-the-dangers-of-the-previous-ground-effect-era.

[11] Formula 1. Lotus 79 [online]. URL: https://www.formula1.com/en/latest/technical/2018/8/tech-tuesday-retro-lotus-79.html.

[12] Greg Stuart. 10 things about the 2022 F1 car [online]. URL: https://www.formula1.com/en/latest/article.10-things-you-need-to-know-about-the-all-new-2022-f1-car.4OLg8DrXyzHzdoGrbqp6ye.html.

[13] Mark Hughes. How the rear wing of the 2022 car has been designed to be an F1 gamechanger [online]. URL: https://www.formula1.com/en/latest/article.tec

h-tuesday-how-the-rear-wing-of-the-2022-car-has-been-designed-to-be-an-f1.70dkHlnyP8DiGDDnMf3tzU.html.

[14] Matt Somerfield. What's changed with F1's new rear wing deflection tests [online]. URL: https://www.motorsport.com/f1/news/whats-changed-with-f1s-new-rear-wing-deflection-tests/10330465/.

[15] Wikipedia. Drag reduction system [online]. URL: https://en.wikipedia.org/wiki/Drag_reduction_system.

[16] Caleb Miller. F1 2022 aerodynamics [online]. URL: https://www.caranddriver.com/news/a37038474/2022-f1-car-revealed/.

[17] Wikipedia. Formula 1 [online]. URL: https://en.wikipedia.org/wiki/Formula_One.

[18] Mercedes AMG F1. Downforce in Formula One, explained [online]. URL: https://www.mercedesamgf1.com/news/feature-downforce-in-formula-one-explained.

[19] theansweris27. Physic models in STAR-CCM+ [online]. URL: https://theansweris27.com/physic-models-in-star-ccm-part-i/.

[20] Comsol. Fully Coupled versus Segregated solution approach [online]. URL: https://www.comsol.com/support/knowledgebase/1258.

[21] LibreTexts. The ideal gas law [online]. URL: https://chem.libretexts.org/Bookshelves/Physical_and_Theoretical_Chemistry_Textbook_Maps/Supplemental_Modules_(Physical_and_Theoretical_Chemistry)/Physical_Properties_of_Matter/States_of_Matter/Properties_of_Gases/Gas_Laws/The_Ideal_Gas_Law.

[22] Simscale. K-Epsilon turbulence model [online]. URL: https://www.simscale.com/docs/simulation-setup/global-settings/k-epsilon/.

[23] Siemens. Physics setup and Solvers in STAR-CCM+ [online]. URL: https://community.sw.siemens.com/s/article/A-new-user-s-guide-to-STAR-CCM-simulation-Part-4-5-Physics-setup-and-Solvers.

[24] theansweris27. Mesh models in STAR-CCM+ [online]. URL: https://theansweris27.com/mesh-models-in-star-ccm/.

[25] Siemens. Meshing in STAR-CCM+ [online]. URL: https://community.sw.siemens.com/s/article/A-new-user-s-guide-to-STAR-CCM-simulation-Part-3-5-Meshing.

[26] Sunu Cherian. Surface remesher in STAR-CCM+ [online]. URL: https://skill-lync.com/student-projects/SURFACE-REMESHER-75700.

[27] Robin Victor. How to use Surface Wrapper Defeature and Contact prevention controls [online]. URL: https://volupe.se/how-to-use-surface-wrapper-defeature-and-contact-prevention-controls/.

[28] Navin Baskar. All about the convergence criteria [online]. URL: https://skill-lync.com/blogs/technical-blogs/cfd-all-about-the-convergence-criteria.

[29] Wikipedia. Nonlinear system [online]. URL: https://en.wikipedia.org/wiki/Nonlinear_system.

[30] Edward T. Gilbert-Kawai, Marc D. Wittenberg. Bernoulli equation and Venturi effect [online]. URL: https://www.cambridge.org/core/books/abs/essential-equations-for-anaesthesia/bernoulli-equation-and-venturi-effect/3316A9D8BAF1D537B0F7AC53E54558DE.

[31] ChemEurope. Vorticity [online]. URL: https://www.chemeurope.com/en/encyclopedia/Vorticity.html.

[32] University of Waterloo. Vorticity [online]. URL: https://uwaterloo.ca/applied-mathematics/current-undergraduates/continuum-and-fluid-mechanics-students/amath-463-students/vorticity.

[33] Wikipedia. Streamlines, streaklines, and pathlines [online]. URL: https://en.wikipedia.org/wiki/Streamlines,_streaklines,_and_pathlines.

[34] The Editors of Encyclopaedia Britannica. Streamline [online]. URL: https://www.britannica.com/science/streamline.